ARMY RESEARCH LABORATORY

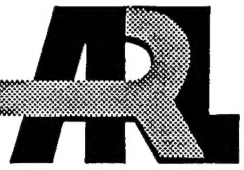

Comparison Between the Scanning Fast-Field Program and Helicopter Data

by John M. Noble
Battlefield Environment Directorate

Michael Barnes
New Mexico State University

ARL-TR-824

December 1995

DISCLAIMER NOTICE

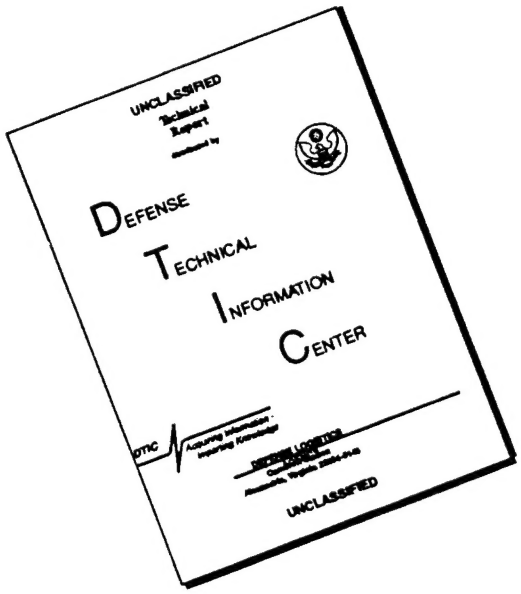

THIS DOCUMENT IS BEST QUALITY AVAILABLE. THE COPY FURNISHED TO DTIC CONTAINED A SIGNIFICANT NUMBER OF PAGES WHICH DO NOT REPRODUCE LEGIBLY.

REPORT DOCUMENTATION PAGE

Form Approved
OMB No. 0704-0188

1. AGENCY USE ONLY *(Leave blank)*	2. REPORT DATE	3. REPORT TYPE AND DATES COVERED
	December 1995	Final

4. TITLE AND SUBTITLE
Comparison Between the Scanning Fast-Field Program and Helicopter Data

5. FUNDING NUMBERS

6. AUTHOR(S)
John Noble and Michael Barns

7. PERFORMING ORGANIZATION NAME(S) AND ADDRESS(ES)
U.S. Army Research Laboratory
Battlefield Environment Directorate
ATTN: AMSRL-BE-S
White Sands Missile Range, NM 88002-5513

8. PERFORMING ORGANIZATION REPORT NUMBER
ARL-TR-824

9. SPONSORING / MONITORING AGENCY NAME(S) AND ADDRESS(ES)
U.S. Army Research Laboratory
2800 Powder Mill Road
Adelphi, MD 20783-1145

10. SPONSORING / MONITORING AGENCY REPORT NUMBER
ARL-TR-824

11. SUPPLEMENTARY NOTES

12a. DISTRIBUTION / AVAILABILITY STATEMENT
Approved for public release; distribution unlimited.

12b. DISTRIBUTION CODE

13. ABSTRACT *(Maximum 200 words)*
A study was conducted to compare the Fast Field Program (FFP) to data from helicopters out to a range of 20 km. The purpose of the study was to observe how the FFP predictions compared to helicopters over ranges out to 20 km and determine if the FFP could reliably be used to predict the propagation conditions for acoustic arrays listening for helicopters. The helicopter data consisted of many passes of a variety of helicopters over a period of several weeks to obtain a large set of data collected under many different acoustic propagation conditions. Simultaneous acoustic and meteorological data was collected during the experiment. The meteorological data consisted of surface observations of relative humidity and pressure with winds measured from the surface to 2 km and the temperature measured from the surface to 400 m. This provided a good set of meteorological data to use as input to the FFP for the comparisons. For most of the comparisons made, the signal-to-noise ratio for the acoustic data was quite good which contributed to the comparison. For the cases where the signal-to-noise ratio was not good, the FFP provided a good comparison until the signal was buried in the noise. The results of the comparison shows that the FFP predictions agreed very well with the trends in the helicopter data.

14. SUBJECT TERMS	15. NUMBER OF PAGES
helicopter, acoustics, FFP, propagation, atmosphere	67
	16. PRICE CODE

17. SECURITY CLASSIFICATION OF REPORT	18. SECURITY CLASSIFICATION OF THIS PAGE	19. SECURITY CLASSIFICATION OF ABSTRACT	20. LIMITATION OF ABSTRACT
Unclassified	Unclassified	Unclassified	SAR

Preface

This report gives a brief discussion on the formulation of the Scanning Fast Field Program (SCAFFIP) and comparison of field data. SCAFFIP is a full wave sound propagation model which incorporates the effects of geometrical spreading, molecular absorption, refraction, acoustically complex ground impedance and diffraction over flat terrain. This model will be used for Tactical Decision and Mission Planning Aids to determine the detectibility of strategic targets by passive acoustic sensor arrays. In order to have confidence in the performance of the model predictions, comparisons between the model and reliable helicopter field data were performed. The helicopter data consisted of several inbound flight paths from 20 km of 1 to 4 helicopters flying over fairly flat terrain. The meteorological data were collected for a series of in situ and remote sensing devices. The meteorological data provided temperature, wind speed and direction from the surface to 2 km. The meteorological data were used as input to SCAFFIP to predict the expected sound levels from each of the helicopter flights. The model predictions were then compared to the actual helicopter sound levers at each of the primary frequencies of the helicopter. The comparison between field data and model shows a very good match between the model prediction and the helicopter data. This means that this model would work very well for predicting sound levels from helicopters over fairly flat terrain for ranges up to 20 km.

Contents

Figures

1. Introduction

The Scanning Fast Field Program (SCAFFIP) is based on the Fast Field Program (FFP) with the added ability to scan multiple azimuths when predicting the propagation conditions about the location of a sensor. The SCAFFIP makes a prediction of the acoustic propagation conditions based on geometrical spreading, molecular absorption, refraction, acoustically complex ground impedance, and diffraction over flat terrain.

The FFP is a one-way solution to the acoustic wave equation originally developed for underwater sound propagation predictions (DiNapoli (1971) and Kutschale (1970)). It was adapted to propagation in the atmosphere by Raspet et al. (1985) and Lee et al. (1986). The FFP developed by Raspet et al. used a propagation matrix formulation. What this means is that if each layer in the atmosphere is viewed as an optical device, then a matrix for each layer in the atmosphere can be constructed. Multiplying each matrix together results in a new matrix that represents how an acoustic signal will be affected as it propagates through the atmosphere. The next step is to take a Bessel Function Transform of the problem with respect to range. After the solution is calculated, an inverse transform is performed to arrive at the final solution.

To determine how well a model predicts reality, the model needs to be evaluated against field data. Some comparisons for this model have already been performed for distances less than 2 km from the source (Frederickson et al. 1993). This report will show how well this acoustic propagation model predicts the sound level from various helicopters flying over relatively flat-earth terrain.

2. Scanning Fast-Field Program

2.1 Speed of Sound

Meteorological phenomena can have a significant effect on the received sound field. Some of the meteorological variables that can affect the speed of sound in air are pressure, temperature, vector wind speed, and humidity. To observe the effect of each meteorological variable considering each independent, lets examine the equation for the speed of sound in air. The value of c, according to Laplace's adiabatic assumption for air as an ideal gas, is (Pierce (1981))

$$c(T) = \sqrt{\frac{\gamma RT}{M}} \tag{1}$$

where γ is the ratio of specific heats, R is the universal gas constant, which is equal to 8314.16 J/(kg K), T is the temperature of air and M is the molecular weight of air.

The presence of water molecules alters the sound speed by lowering γ and decreasing M. The decrease in M dominates so that the overall effect of increasing humidity is an increasing sound speed. These changes can be quantified as

$$\gamma = \frac{7 + h}{5 + h} \tag{2}$$

$$M = 29 - 11h \tag{3}$$

where h is the fraction of water molecules in air. As the amount of water in the atmosphere increases, the molecular weight of air will decrease since the molecular weight of a water molecule is less than diatomic nitrogen. This effect will try to increase the sound speed as the fraction of water molecules in the air increases. In order to calculate the fraction of water molecules in air, the Goff-Gratch equation (equation (4)), must be used to first calculate the partial pressure of saturated water vapor, P_{sat} at temperature T.

$$\begin{aligned} \log_{10}\left(\frac{P_{sat}}{P_o}\right) = {} & 10.79586\left[1 - \left(\frac{T_{01}}{T}\right)\right] - 5.02808\log_{10}\left(\frac{T}{T_{01}}\right) + \\ & 1.50474 \times 10^{-4}\left(1 - 10^{-8.29692\,[(T/T_{01})-1]}\right) + \\ & 0.42873 \times 10^{-3}\left(10^{4.76955\,[1-(T_{01}/T)]} - 1\right) - 2.2195983 \end{aligned} \tag{4}$$

where T_{01} = 273.16°K and p_o = 1 atm which is the reference pressure. Upon arriving at a value for P_{sat}, the fraction of water molecules in air can be calculated using the following relationship

$$h = \frac{10^{-2}(RH)\,P_{sat}}{P} \tag{5}$$

where RH is the relative humidity in percent and P is the pressure in atmospheres.

The magnitude of the dependence of the sound speed on humidity is not obvious. To understand the degree of the effect of humidity on sound speed, consider a particular case. At 20 °C, the difference in sound speed between 0 and 100 percent humidity is 2 m/s. A fluctuation in the humidity of this amount is very unlikely. If the variation in humidity is reduced to a change of 50 to 100 percent, the change in the sound speed is only 1 m/s. Therefore, the variation of sound speed due to changes in humidity should always be much less than 1 m/s. Generally, humidity fluctuations can be ignored.

The effect of the wind speed on the speed of sound is a vector relation. The effective sound speed is calculated using

$$c_{eff} = c(T) + u \cdot \cos(\theta_w - \pi - \theta_R) \tag{6}$$

where c(T) is the speed of sound in the absence of wind at temperature T, u is the magnitude of the horizontal wind speed, θ_R is the bearing of the receiver from the source, θ_w is the direction from which the wind blows, and $\theta_w - \pi$ is the direction the wind is blowing (figure 1). All directions are relative to the north.

Since the sound speed is primarily a function of temperature and vector wind speed, the sound speed will also vary with height. This will cause the acoustic wave to be refracted as it propagates through the atmosphere. The degree of refraction the acoustic wave undergoes is related to the sound speed gradient present in the atmosphere. If the sound speed increases with height, the acoustic wave will be refracted downwards. If the sound speed decreases with height, the acoustic wave will be refracted upwards.

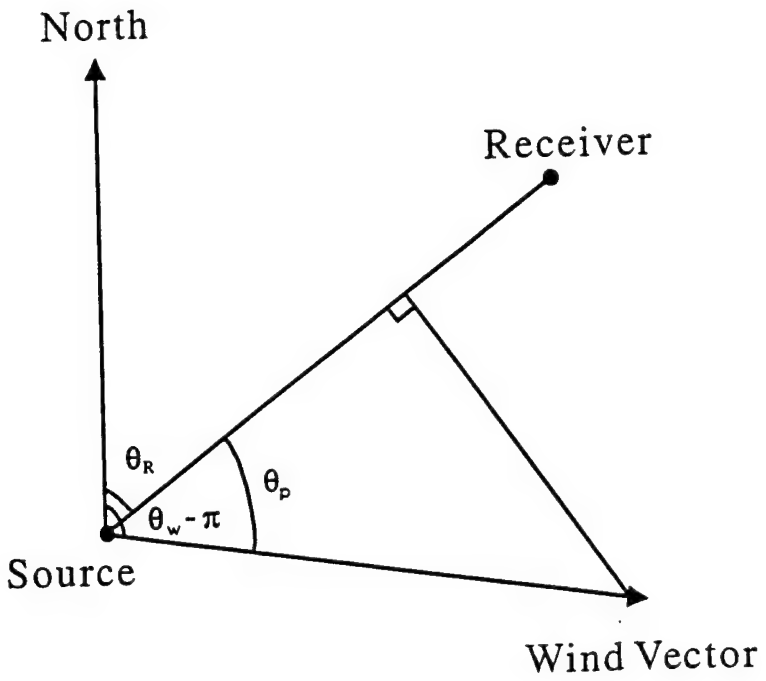

Figure 1. Diagram of geometry definition.

2.2 Fast Field Program

The propagation of sound from a point source located at the origin is given by the classical wave equation

$$\nabla^2 p - \frac{1}{c^2}\frac{\partial^2 p}{\partial t^2} = -4\pi\,\delta(x,y,z) \tag{7}$$

where δ represents a delta function source of unit strength. For simple harmonic motion, equation (7) becomes the Helmholtz equation

$$\nabla^2 p + k^2 p = -4\pi\,\delta(x,y,z) \tag{8}$$

where k = ω/c is the wavenumber, c is the sound speed, and ω is the angular frequency. For the FFP, k and c are restricted to vary only in the z-direction.

Transforming equation (8) into cylindrical coordinates and assuming azimuthal symmetry, the Helmholtz equation becomes

$$\frac{\partial^2 p}{\partial r^2} + \frac{1}{r}\frac{\partial p}{\partial r} + \rho \frac{\partial}{\partial z}\left(\frac{1}{\rho}\frac{\partial p}{\partial z}\right) + k^2 p = -\frac{2}{r}\delta(r)\,\delta(z-z_s) \qquad (9)$$

where the source is located at r = 0 and z = z_s and ρ is the density of the medium.

For the FFP, the atmosphere is viewed as a series of constant sound speed layers as shown in figure 2. The layers in the atmosphere are bounded on top and bottom by complex impedance surfaces. The top boundary is typically modeled as an infinite half-space with constant parameters. At the bottom boundary, the atmospheric layer adjoins a partially absorbing surface which can be represented by the complex acoustical impedance of the ground.

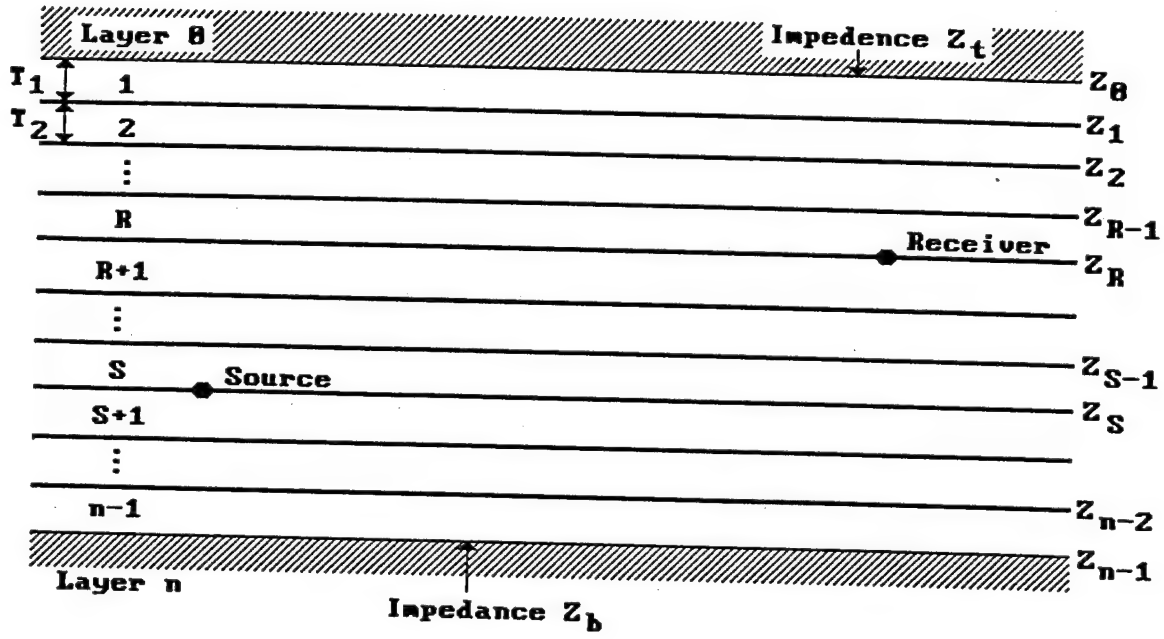

Figure 2. Layering of the atmosphere by the FFP.

To reduce the dimensionality of equation (9), a zero-order Hankel transform is applied with respect to the range variable r. This gives the transform pair:

$$\check{p}(\kappa,z) = \int_o^\infty p(r,z)\, J_o(\kappa r)\, r\, dr$$

$$p(r,z) = \int_o^\infty \check{p}(\kappa,z)\, J_o(\kappa r)\, \kappa\, d\kappa \qquad (10)$$

Applying the first transform to equation (9) results in

$$\frac{d^2\check{p}}{dz^2} + [\,k^2(z) - \kappa^2\,]\,\check{p} = -2\,\delta(z-z_s) \qquad (11)$$

This equation can be decomposed into

$$\check{u}_z = \frac{i}{\omega\,\rho_o}\,\frac{d\check{p}}{dz} \qquad (12)$$

$$\frac{d\check{u}_z}{dz} = \frac{i}{\omega\,\rho_o}\,\frac{d^2\check{p}}{dz^2} = -\frac{i}{\omega\,\rho_o}\,[\,k^2(z) - \kappa^2\,]\,\check{p} + \frac{2}{i\,\omega\,\rho_o}\,\delta(z-z_s) \qquad (13)$$

where ρ_o is the mean air density and $\check{u}_z$ is the transformed particle velocity in the z-direction. The delta function is the source term producing a discontinuity in $\check{u}_z$ at a height z_s. In order to solve the resulting equations, Lee et al. (1986) used an analogy to a transmission line which results from the form of the transformed equation. The transformed equations have a very similar form to the "Telegrapher's Equations" of electrical transmission line theory.

Using this analogy, the acoustic problem can be arranged so that a solution can be calculated. The analogy is made by representing each layer in the atmosphere by an element in a transmission line with a certain characteristic admittance and attenuation constant. The admittance is defined as one over the impedance or one over the sum of the resistance plus reactance of the electrical element. The admittance of the element cause the voltage running through it to be attenuated and a shift in the phase of the signal. Viewing it from the perspective of the acoustic wave problem, the acoustic wave as it is propagated through the atmosphere undergoes losses and phase shifting due to refraction and spreading of the acoustic wave. This equivalence can be carried out for each layer of the atmosphere thus constructing a transmission line. The top and bottom boundaries in the atmosphere becomes loading admittance elements on each end of the transmission line. Now the problem has been converted from determining the voltage in the transmission line at a point in the line. This is a well known process in electrical engineering.

The zero-order Bessel function in equation (10) can be expanded using Hankel functions:

$$J_o(\kappa r) = \frac{1}{2}\left[H_o^{(1)}(\kappa r) + H_o^{(2)}(\kappa r)\right] \tag{14}$$

The Hankel functions can be represented as an incoming and outgoing acoustic wave. The FFP is designed to model radially outgoing acoustic waves. This allows for the first Hankel function to be suppressed with the additional argument that the incoming acoustic wave will not contribute significantly to the final result. The asymptotic expansion of the second Hankel function for large arguments,

$$H_o^{(2)}(\kappa r) \approx \sqrt{\frac{2}{\pi\kappa}}\,\frac{e^{-i(\kappa r - \pi/4)}}{\sqrt{r}} \qquad \kappa r \gg 1 \tag{15}$$

makes the problem easier to handle. The important contributions from the integrand of the inverse transform, equation (10), comes from the area where $\kappa \sim k_o$. Substituting equation (15) into the inverse transform of equation (10) and taking the far-field approximation, the acoustic pressure equation can be written as

$$p(r,z_r) \approx \frac{(1+i)}{2\sqrt{\pi r}} \int_0^{\infty} \breve{p}(\kappa,z_r)\, e^{-i\kappa r}\sqrt{\kappa}\, d\kappa \qquad (16)$$

In order to perform the calculation on a computer, the continuous integral must be replaced by a numerical integral over discrete values of κ. Applying this to equation (16) yields:

$$p(r,z_r) = \frac{(1+i)}{2\sqrt{\pi r}}\, \Delta\kappa \sum_{n=0}^{N-1} \breve{p}(\kappa_n)\sqrt{\kappa_n}\; e^{-i\,(2\pi nm/N)} \qquad (17)$$

where

$$\Delta\kappa = \frac{\kappa_{max}}{N-1} \qquad \kappa_n = n\Delta\kappa$$
$$m = \frac{r}{\Delta r} \qquad \Delta r = \frac{2\pi}{N\Delta\kappa} \qquad (18)$$

The term κ_{max} comes from the property of the integrand of equation (10) only has significant contributions in a finite range of κ. This allows the summation to be terminated at a finite number of terms.

2.3 Absorption of Sound in the Air

Losses in the medium are basically caused by viscosity, heat conduction, and molecular exchanges of energy. In the nineteenth century, the mechanisms of viscosity and heat conduction were the only ones suspected of causing dissipation of sound. Therefore, they are presently referred to as classical absorption.

In classical absorption, if one represents the effect of absorption by a factor $e^{-\alpha r}$ where r is the distance of propagation, then the attenuation coefficient α_{cl} due to viscosity and heat conduction is given by equation (17) from *Physical Acoustics XVII* (Academic Press, New York (1984)

$$\alpha_{cl} = 5.578 \times 10^{-9} \frac{T/T_o}{T + 110.4} \frac{f^2}{P/P_o} \tag{19}$$

The units of α_{cl} in equation (19) are nepers/meter,

where

P_o = Reference pressure of 1.01325 X 10^5 N/m^2 (1 atm)
P = Atmospheric Pressure in N/m^2
T_o = Reference temperature of 293.15° K
T = Temperature in °K
f = Frequency (Hz)

In molecular absorption, energy exchanges at the molecular level include rotational and vibrational modes. Analysis of the rotational mode shows that its representative attenuation coefficient is proportional to α_{cl}, the classical attenuation coefficient:

$$\frac{\alpha_{rot}}{\alpha_{cl}} = 4.16\, e^{-16.8 T^{-1/3}} \tag{20}$$

when 293° K < T < 690° K.

For frequencies below 10 MHz, it has been demonstrated that energy losses due to classical and molecular absorption are additive.

$$\alpha_{cr} = \alpha_{cl} + \alpha_{rot} \tag{21}$$

A simplified empirical form of the equation can be written

$$\alpha_{cr} = 1.83 \times 10^{-11} \frac{\sqrt{T/T_o}\, f^2}{P/P_o} \tag{22}$$

which is correct within 2 percent for 213° K < T < 373° K.

There remains to consider the vibrational mode of absorption. Since the atmosphere is made up mostly of nitrogen and oxygen, each will contribute an attenuation coefficient,

$$\alpha_{vib,\,j} = \frac{4pX_j}{35c}\left(\frac{q_j}{T}\right)^2 \frac{e^{-q_j/(Tf^2)}}{f_{r,\,j} + (f^2/f_{r,\,j})} \tag{23}$$

where j stands for either oxygen or nitrogen. The symbols are defined as follows:

X_j = Mole fraction of air component considered (0.20948 for oxygen and 0.78084 for nitrogen).

q_j = Characteristic vibrational temperature (2239.1° K for oxygen and 3352.0° K for nitrogen).

c = Speed of sound at temperature T (m/s).

The $f_{r,j}$ are the individual relaxation frequencies for oxygen and nitrogen. The computation of these depends on the relative humidity and atmospheric pressure. The relaxation frequencies are given by:

$$f_{r,O} = \frac{P}{P_o}\left(24 + 4.04\,x\,10^4 h\,\frac{0.02 + h}{0.391 + h}\right)$$

$$f_{r,N} = \frac{P}{P_o}\sqrt{\frac{T_o}{T}}\left(9 + 280\,he^{-4.170\,(T_o/T)^{1/3}-1}\right) \tag{24}$$

The total attenuation coefficient is then the sum of α_{cr} and $\alpha_{vib,j}$. Figure 3 is a log-log plot (Franke and Swenson (1989) of total attenuation coefficient for T = 20 °C and Rh = 20 percent. Figure 3 shows the attenuation due to classical absorption, vibrational relaxation of Nitrogen and Oxygen, and the total attenuation coefficient due to the sum of the three attenuation mechanisms.

The attenuation coefficient α is proportional to the square of the frequency. As the frequency doubles, the attenuation will quadruple. The attenuation of the sound wave due to molecular and vibrational absorption is very important for frequencies over 250 Hz. For frequencies below 250 Hz, this attenuation does not contribute much to the total attenuation of the sound wave.

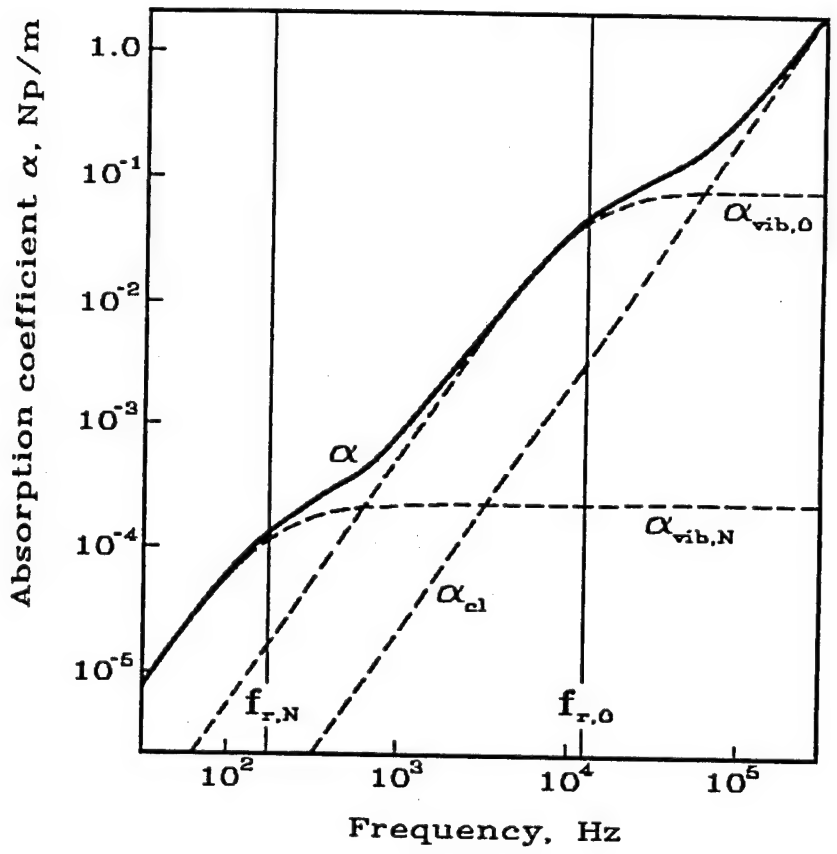

Figure 3. Log-log plot of sound-absorption coefficient versus Frequency for sound in air at 20 °C at 1 atm pressure and with a water-vapor fraction h of 4.676×10^{-3} (Rh = 20 percent).

2.4 Complex Ground Impedance

There are several models available for calculating the complex ground impedance. The impedance model used in SCAFFIP is the Four Parameter Model of Attenborough (1985). In this impedance model, the complex normalized characteristic impedance of the ground is calculated using:

$$Z_c \cong \frac{\left[\frac{4q^2}{3\Omega} + i\frac{S_f^2 \sigma}{\omega \rho_o}\right]}{k_b} \tag{25}$$

where

q^2 = $\Omega^{-n'}$
S_f = the pore shape factor ratio,
Ω = the porosity of the ground,
σ = the flow resistivity of the ground (mks) rayls,
ω = the angular frequency,
ρ_o = the density of air (1.2 kg/m^3), and
k_b = the normalized wave number.

The normalized wave number k_b is computed from

$$k_b \cong \sqrt{\gamma \Omega}\left[\left(\frac{4}{3} - \frac{\gamma - 1}{\gamma} N_{pr}\right)\frac{q^2}{\Omega} + i\frac{S_f^2 \sigma}{\omega \rho_o}\right]^{1/2} \tag{26}$$

where γ is the ratio of specific heats, equation (2), and N_{pr} is the Prandtl number (0.724).

The parameters S_f, Ω, ρ_o, and n' are normally varied until agreement is reached between impedance measurements and the impedance model is achieved. However, this method of determining the four parameters cannot always be completed if time or resources is lacking. The parameters used in this comparison were measured in the area where the helicopter data was collected.

Some ground surfaces have a layered structure which results from the gradual deposition of material over a soil base. For example: a layer of snow over frozen ground, decomposition of organic material over clay or sandy soil, or a well plowed pasture over clay or harder packed soil. An effective impedance Z(d) can be calculated for a semi-infinite layer of impedance Z_2 covered by a layer, depth d, of another material of impedance Z_1. The effective impedance is given by

$$Z(d) = \left[\frac{Z_2 - iZ_1 \tan(k_b d)}{Z_1 - iZ_2 \tan(k_b d)} \right] Z_1 \qquad (27)$$

where k_b is the bulk propagation constant in the top layer of the ground. The parameters Z_1, Z_2, and k_b are calculated using equations (25) and (26) from Attenborough's Four Parameter impedance model.

3. Experimental Setup

The experiment was conducted at SHORAD test site located on McGregor Range near Orogrande, NM, 50 miles northwest of El Paso, TX. The test was composed of several types of helicopters each flying in toward the test site along various paths at different speeds. To simplify the comparison, two types of helicopters were used in the comparison flying along the paths and speeds shown in Appendix B. This path was chosen because the helicopter flew almost straight at the sensor and the terrain along most of the flight path is fairly flat. Part of the measurements were made over irregular terrain, however, that part of the experiment will be analyzed at a later date when a model is available for predicting the effects of terrain. The helicopters were tracked with a radar system to know the location of the helicopter at any point in time during the test flight. Data runs consisted of 1 to 4 helicopters flying from 20 km out in range to the sensor location.

3.1 Acoustic Sources

There was a total of eight types of helicopters used for the field trials. The helicopters were flown under seven flight paths. Each flight path was flown at 3 heights and 2 speeds under a variety of atmospheric conditions. This provides a very large database of helicopter data to choose from. To simplify the comparison, two types of helicopters were used in the

comparison for this report flying one flight path under a variety of atmospheric conditions. This was done to minimize the variability of the source over the flight path. Helicopters can be a highly variable source, since the sound level changes as the helicopter alter height and direction. The flight path chosen for the comparison is straight in approach at a constant height and speed. The typical flight path used in the comparison is shown in figure 4.

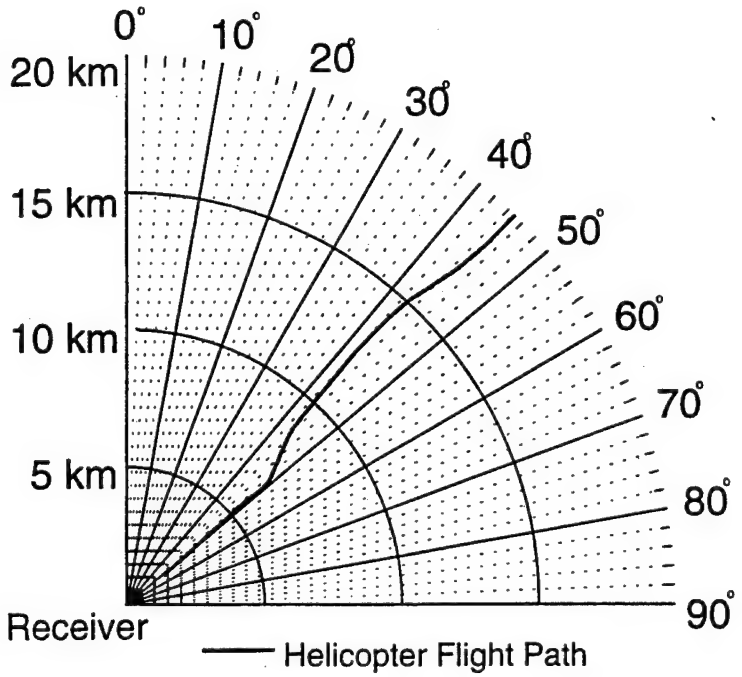

Figure 4. Typical flight path for the helicopters.

3.2 Acoustic Receivers

The acoustic array consisted of six microphones arranged in a simple box array format (figure 5), with four microphones comprising the corners of the box and two microphones located at the center of the box. The microphones used were B&K 4166 microphones with a low frequency cutoff of 2.6 Hz and a high frequency cutoff of 10 kHz. The microphones were bandpassed through Tektronix AM 502 Differential Amplifiers with a bandpass of 0.1 Hz to 1 kHz. Since the acoustic source was helicopters, most of the acoustic energy is in the region between 10 and 500 Hz. The acoustic data was recorded on a Teac RD-200T PCM data recorder running in 6 channel mode giving a bandwidth of DC to 5 kHz.

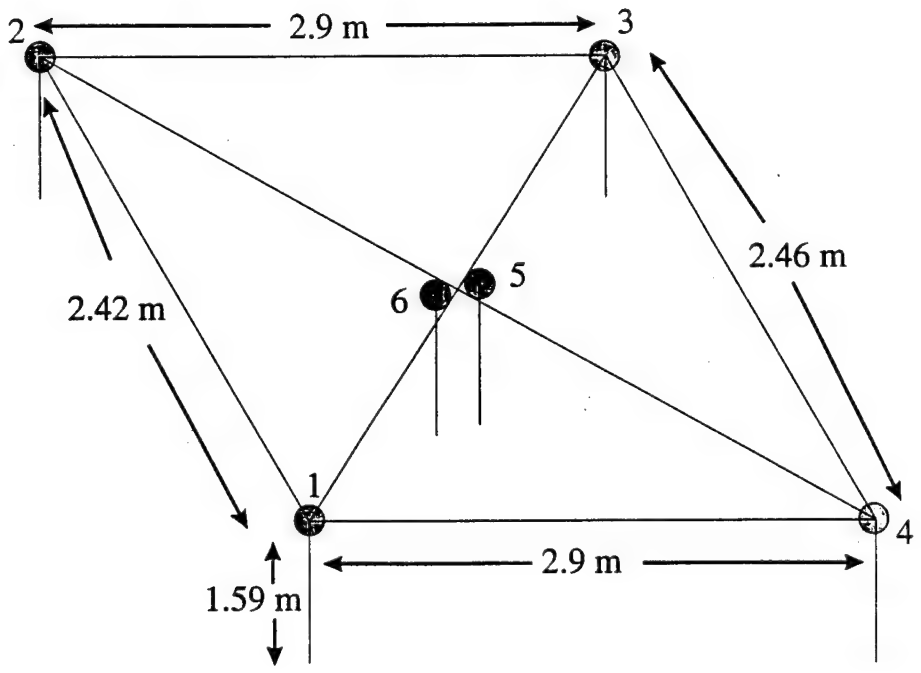

Figure 5. Geometry of the microphone array used in the field test.

3.3 Tracking of Acoustic Sources

The helicopters where tracked using Multiple Target Tracking System (MTTS). The MTTS is a radar-based tracking system that provided UTM coordinates for the helicopters during each flight at an interval of 0.1 s. Using the survey point at the receiving array, this allows for knowing the relative range and direction of the helicopter from the array. Since the sound that was detected by the acoustic array was produced by the source at an earlier time, the position data had to be corrected for the travel time between the source and the array. This was done by using the meteorological data to calculate the travel time between the source and the array. The detection time was corrected by the travel time of the acoustic wave to obtain the position of the helicopter at the true time the sound was emitted.

3.4 Meteorological Data

The meteorological data was collected from a number of sensors collocated with the microphones. A 10 m tower provided temperature, wind speed, wind direction, and humidity at 2 and 10 m and atmospheric pressure at 2 m. A 924 Mhz wind profiling radar was used to obtain wind speed and wind direction from 100 m to 2 km with a height resolution of 100 m with a 15 min average every 20 min. A Radio Acoustic Sounding System (RASS) provided temperature readings from 100 m to 500 m with a height resolution of 150 m with a 5 min average every 20 min. The averaging intervals for the profilers are such because the wind profiling radar was used to operate the RASS. The temperature data was interpolated or extrapolated to the heights for the wind profiling radar. The two relative humidity readings were averaged and used for all the heights. This gave a meteorological profile from the surface to 2 km for each run of the helicopter(s). The meteorological profiles and the sound speed along the mean bearing are presented in Appendix A.

4. Comparison

In order to perform the comparisons, the acoustic propagation model had to be setup to run each case. Since the flight path of the helicopter was not always constant in direction, the relative sound pressure level with range was calculated along several azimuths. The helicopter path was used to

interpolate among the azimuths to determine the relative sound pressure with range along the actual flight path of the helicopter for each pass. The value for the ground impedance was calculated from Attenborough (1985) using ground parameters measured the year before by Keith Attenborough and Henry Bass. The height of the helicopter was obtained from the radar tracking data. Using this information and the closest meteorological profile in time of the run, the SCAFFIP was used to calculate the relative sound pressure level along the flight path. Since the output of the SCAFFIP is the relative attenuation from 0 dB at 1 m of the sound field with range, the SCAFFIP output had to be adjusted to the field data by performing a "best fit" to the field data since there was no value available for the source strength at each of the frequency peaks at 1 m.

The data was analyzed using an HP 35660A signal analyzer. The data was averaged over a period of 15 s. Through the analysis of the acoustic data, the frequencies to run the model was chosen from the main and tail rotor blade peaks and their respective harmonics. The position of each of the data points was corrected for the travel time of the acoustic wave from the helicopter to the receiver to obtain the true position of the helicopter over the flight path. The background noise levels were measured to ensure that the data was valid. Run 4 will show what happens when the received acoustic signal drops below the background noise level.

4.1 Run 1

Figure C.1 shows the comparison between the SCAFFIP and field data for run #1 at a frequency of 21 Hz. It contains the characteristic decrease of the sound level with range. The SCAFFIP shows very good agreement with the data out to 14 km where the signal from the helicopter was lost. The sound speed profile is shown in figure A.4. It shows a characteristic acoustic ducting region within the first 300 m of the atmosphere due to a wind shear at that height. This allows for the good propagation conditions resulting in propagation out to 14 km. Figure C.2 shows the comparison between the SCAFFIP and field data for run #1 at a frequency of 124 Hz. The higher frequency still shows good comparison of SCAFFIP to the field data with similar trends in the data and model between 6 and 8 km.

4.2 Run 2

Run #2 was made on the same day as run #1, but run #2 was 1.5 h later. The sound speed profile (figure A.8), shows the slope in the lower part of the duct is almost zero. This is due to the increase in the temperature lapse rate near the surface from run #1. However, the ducting region is still present with the vertical extent of the duct to 400 m. Figure C.3 shows the comparison between SCAFFIP and field data for run #2 at a frequency of 21 Hz. The model performs well when compared to the data out to 17 km. At about 17 km, the data continues to decrease while the model increases. In the discussion of the next data run, an explanation will be provided why this discrepancy is present. Looking at the 124 Hz data, the comparison between the model and data is very good (figure C.4).

4.3 Run 3

Run #3 was made on another day from runs #1 and #2. Figure A.12 shows the sound speed profile for run #3. The sound speed profile is similar to the other two, but there are some distinct differences between them. The lower region of the ducting area is upward refracting instead of homogeneous or downward refracting. This initially causes sound propagating from the source to propagate upward, possibly forming a shadow zone region. Looking at the comparison between model and data (figure C.5), there is a very good fit between the SCAFFIP and the field data. However, there are two interesting items not in the comparison but in the behavior of the data and the model. Examining the previous two runs, the mean slope of the sound levels with range decrease as the source is further from the sensors as would be expected from spreading losses. However, the decrease of the sound levels with range for run #3 is almost zero. This means that beyond a certain distance, the sound wave is not attenuated very much. This characteristic is supported by both the model and the data. The signal-to-noise ratio for this run is well above the noise floor indicating that the data are valid for this run out to 20 km. Something very interesting is occurring in this case which is limiting the rate of energy loss with range for the acoustic signal. Looking at the higher frequency comparison (figure C.6), the low attenuation with range is still present and the model does a good job in predicting this behavior. Although the helicopter used in this comparison is different from the previous two comparisons, this type of behavior was not observed in other runs made with this helicopter on other days. So this behavior is not due to using another helicopter. As in run #2, there is a

deviation between model and data starting about 17 km in range for the low frequency comparison. After examining several possible reasons, the best reason for the deviation between the model and the data is due to height resolution of the meteorological data used in the comparison. Noticing the results of other work with the SCAFFIP, it was noted that problems could occur if the height resolution of the meteorological profile was to low. Going back to the meteorological profile and performing a linear interpolation to increase the height resolution resulted in the deviation at 17 km for runs #2 and #3 to be corrected, as seen in figures 6 and 7. This effect is not as evident in the higher frequencies due to the constructive and destructive interference patterns cause large variations in the signal. If the large variations are averaged out, the higher frequencies show a similar behavior at the 17 km point. The results of this finding are being incorporated into future versions of the SCAFFIP.

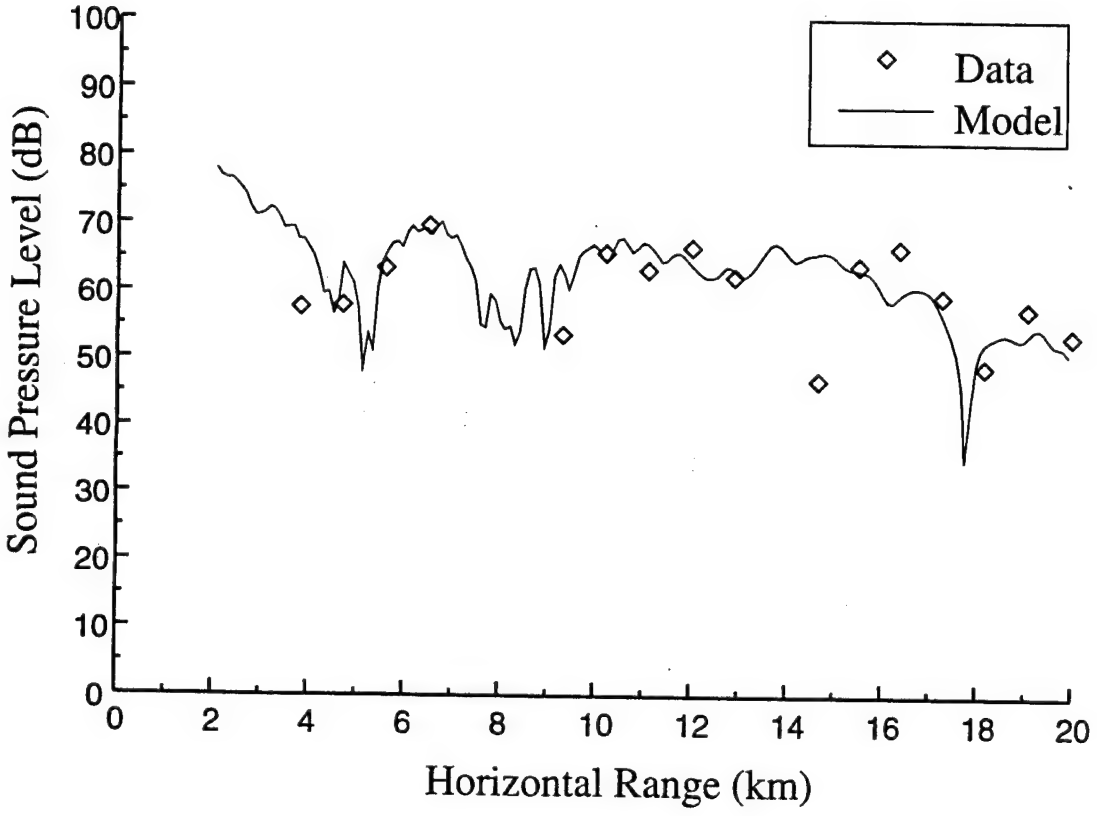

Figure 6. Run #2 at 21 Hz using finer grid spacing of the meteorological profile.

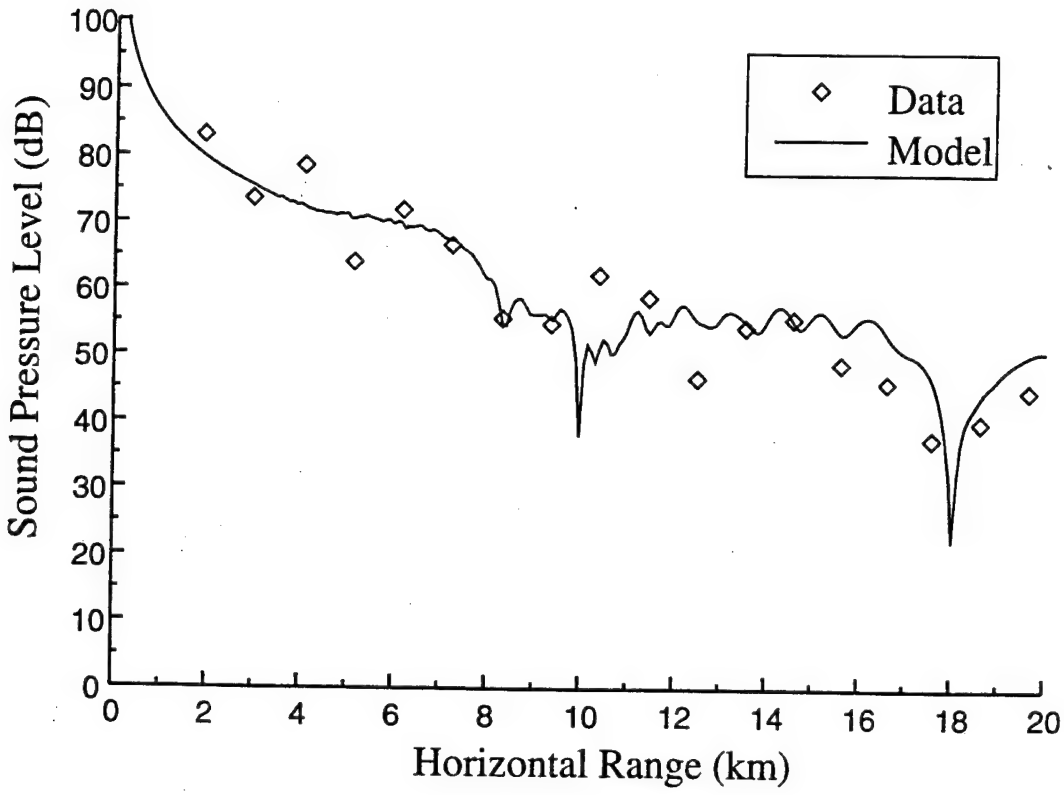

Figure 7. Run #3 at 23 Hz using finer grid spacing of the meteorological profile.

4.4 Run 4

Run #4 was also executed on a different day from the previous three runs. However, this run consisted of both types of helicopters used in the previous runs. This allowed for a side by side comparison for both types of helicopters under the same atmospheric conditions. The sound speed profile for this run is shown in figure A.16. As in the previous runs, there is a duct present extending to 500 m allowing for long range propagation. This run also showed very good comparisons between the model and the helicopter data where good signal-to-noise were present (figures C.7 through C.10). Figure 8 shows the model performed very well until 10 km out when the signal dropped below the noise floor.

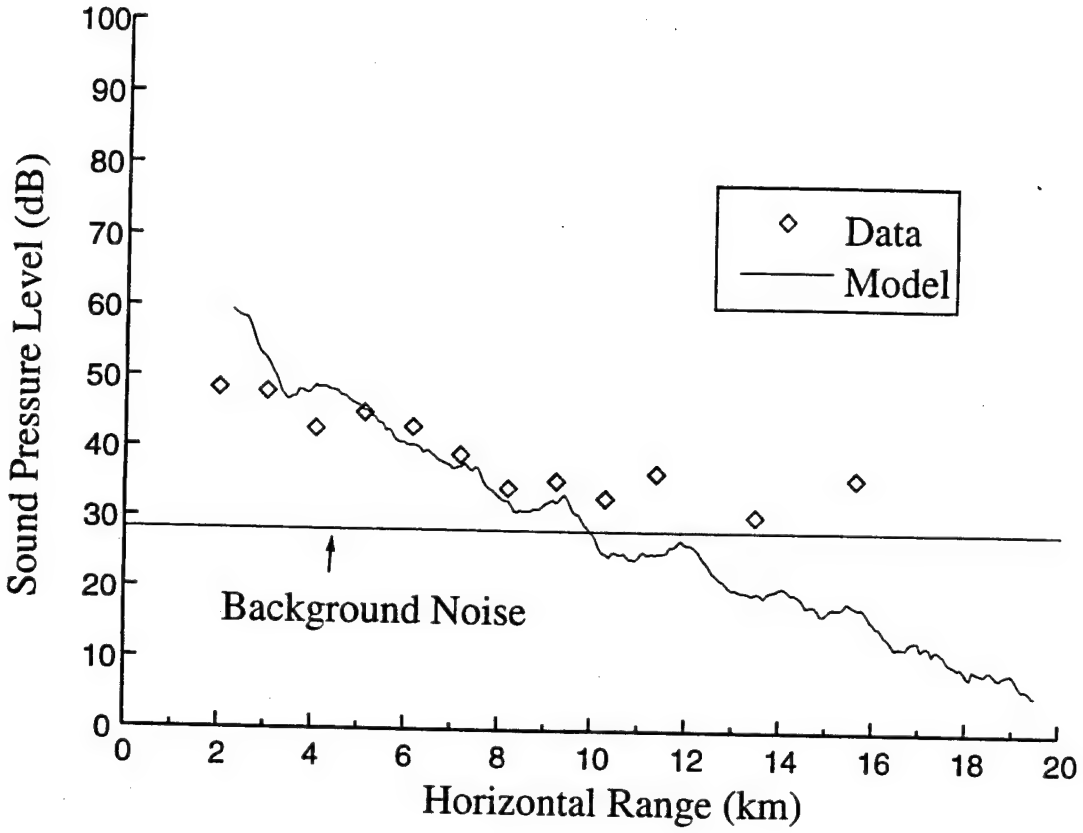

Figure 8. Run #4 at 165 Hz showing signal dropping below background noise.

5. Summary

A comparison was conducted to evaluate the performance of using the SCAFFIP for predicting the sound attenuation at ranges up to 20 km for helicopters. The data was collected for a variety of helicopters flying from 20 km toward the sensor under a variety of atmospheric conditions. The SCAFFIP was used to calculate the attenuation of the sound along the helicopter's flight path and comparing the model output to the field measurements. The comparison was restricted to helicopter flight paths over flat-earth since the SCAFFIP does not have terrain incorporated into it. A total of 6 runs were used in the comparison with each run consisting of approximately 11 frequencies ranging from 10-200 Hz. The SCAFFIP results showed very good predictions when compared to the field data for a variety of frequencies where the signal-to-noise ratios were good . The data also showed some interesting behavior in one of the comparisons. For Run #3, the model and the data showed very little attenuation with range. This is a good indication that the model is predicting the correct effects present in the atmosphere. The conclusion from this comparison, SCAFFIP with helicopter field data, is SCAFFIP is doing a good job predicting the attenuation of sound from helicopters out to 20 km over fairly flat terrain.

References

Attenborough, K., "Acoustical Impedance Models For Outdoor Surfaces," J. Sound Vib **99** (1985), 521-544.

DiNapoli, F. D., A fast field program for multilayered media. Naval Underwater Systems Center, Tech. Report 4103, 1971.

Franke, S. J., and G. W. Swenson, Jr., "A Brief Tutorial on the Fast Field Program (FFP) as Applied to Sound Propagation in the Air," Applied Acoustics 27 (1989) 203-215.

Frederickson, Carl, Henry Bass, Richard Raspet, and John Messer, "Comparison of Measured and Predicted Pure Tone Propagation Levels From JAPE-1: An Evaluation of the Performance of ASOPRAT," Proc. of the Joint Acoustic Propagation Experiment (JAPE) Workshop, Hampton, Virgina, 1993.

Kutschale, H. W., The integral solution of the sound field in a multilayered liquid-solid half-space with numerical computations for low-frequency propagation in the Arctic Ocean. Report No. 1(CU1-1-70, ONR Contract N00014-67-A-0108-0016), Lamont-Doherty Geological Observatory, Columbia University, Palisades, New York, 1970.

Lee, S. W., N. Bong, W. F. Richards, and R. Raspet, "Impedance formulation of the fast field program for acoustic wave propagation in the atmosphere," J. Acoust. Soc. Am. **79** (1986) 628-634.

Physical Acoustics XVIII, edited by Mason and Thurston (Academic Press, New York, 1984), pp. 145-232.

Pierce, Allen D., *Acoustics: An Introduction to Its Physical Principles and Applications* (McGraw-Hill Book Company, New York, 1981).

Raspet, R., S. W. Lee, E. Kuester, D. C. Chang, W. F. Richards, R. Gilbert, and N. Bong, "Fast-field program for a layered medium bounded by complex impedance surfaces," J. Acoust. Soc. Am. 77 (1985) 345-352.

Acronyms and Abbreviations

ARL/BED	U.S. Army Research Laboratory Battlefield Environment Directorate
CERL	U.S. Army Construction Engineering Research Laboratory
FFP	Fast Field Program
MTTS	Multiple Target Tracking System
RASS	Radio Acoustic Sounding System
SCAFFIP	Scanning Fast Field Program
SHORAD	
UTM	

Appendix A

Meteorological and Sound Speed Profiles For Each Comparison

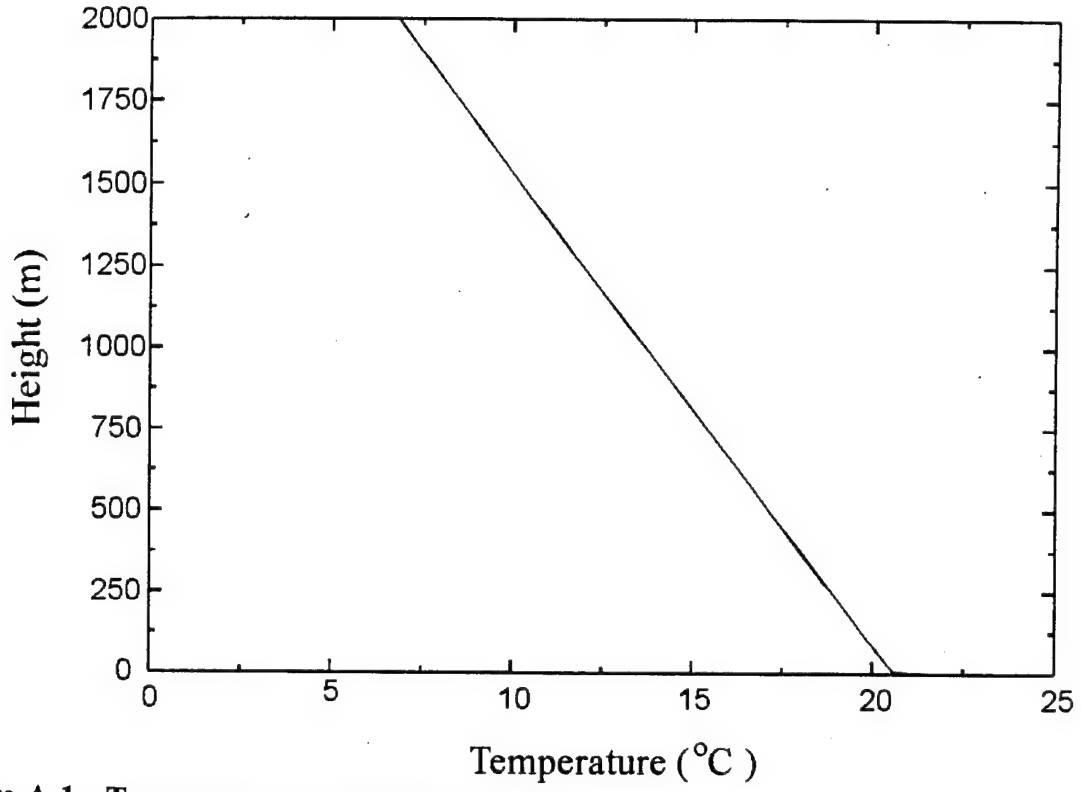

Figure A-1. Temperature profile for Run #1.

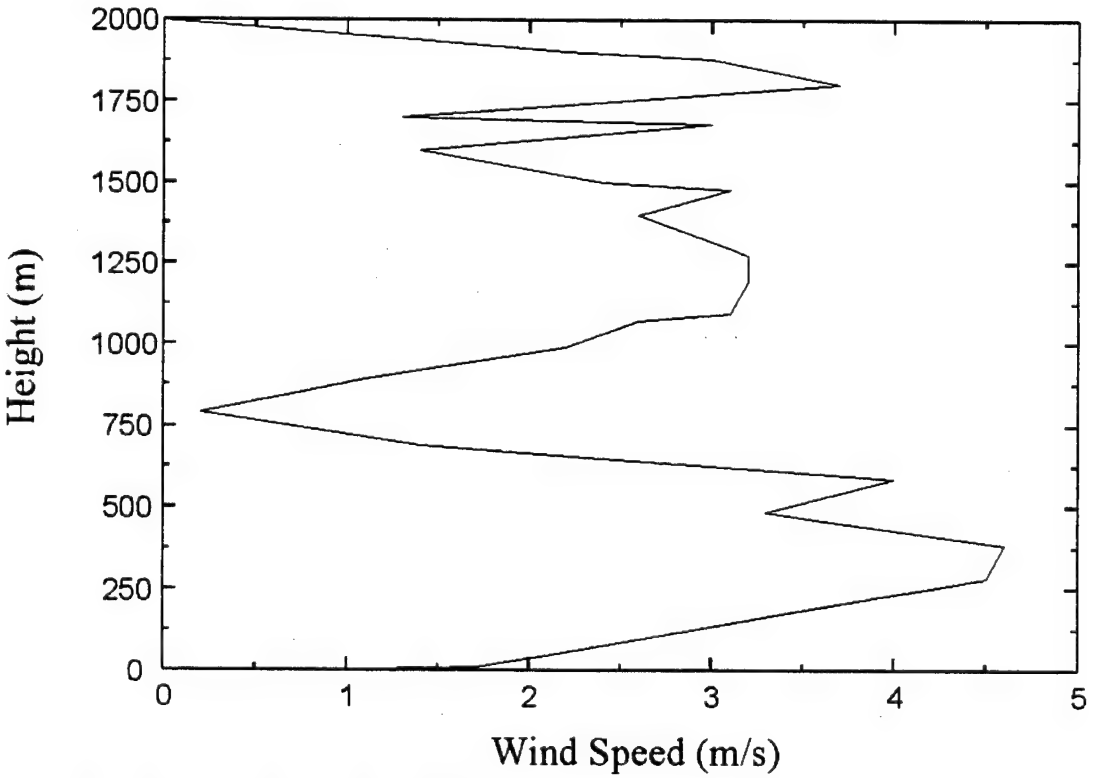

Figure A-2. Wind speed profile for Run #1.

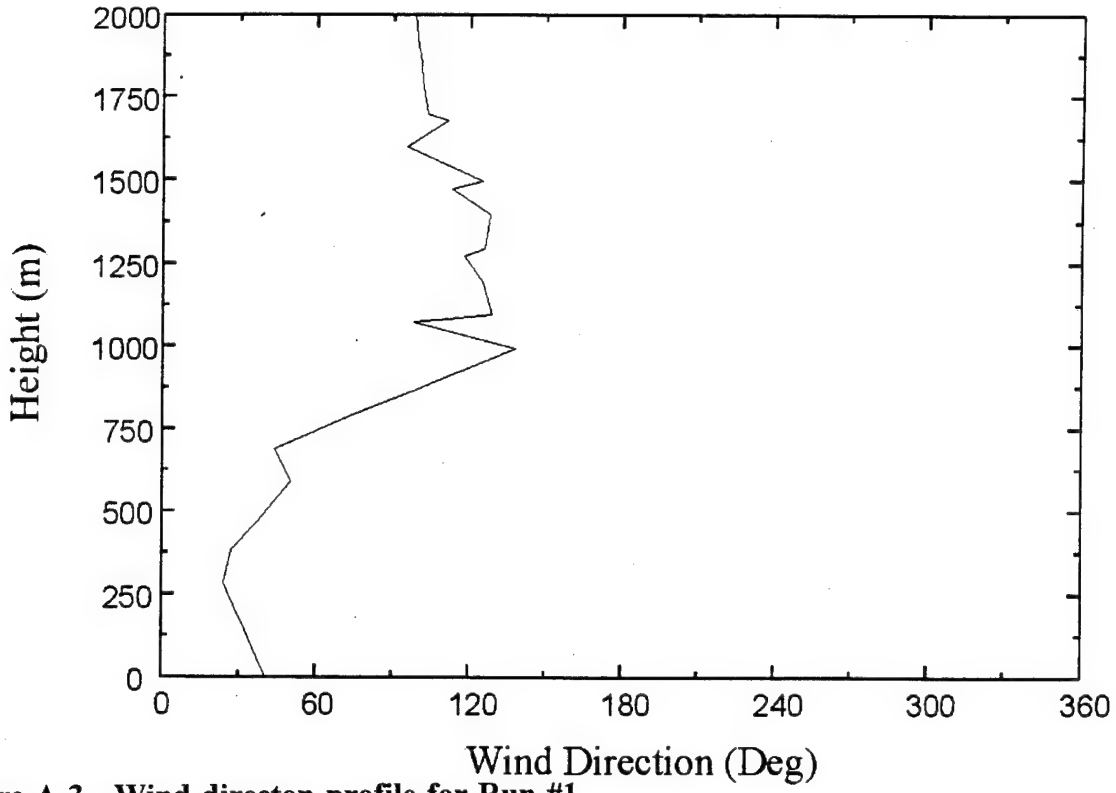

Figure A-3. Wind directon profile for Run #1.

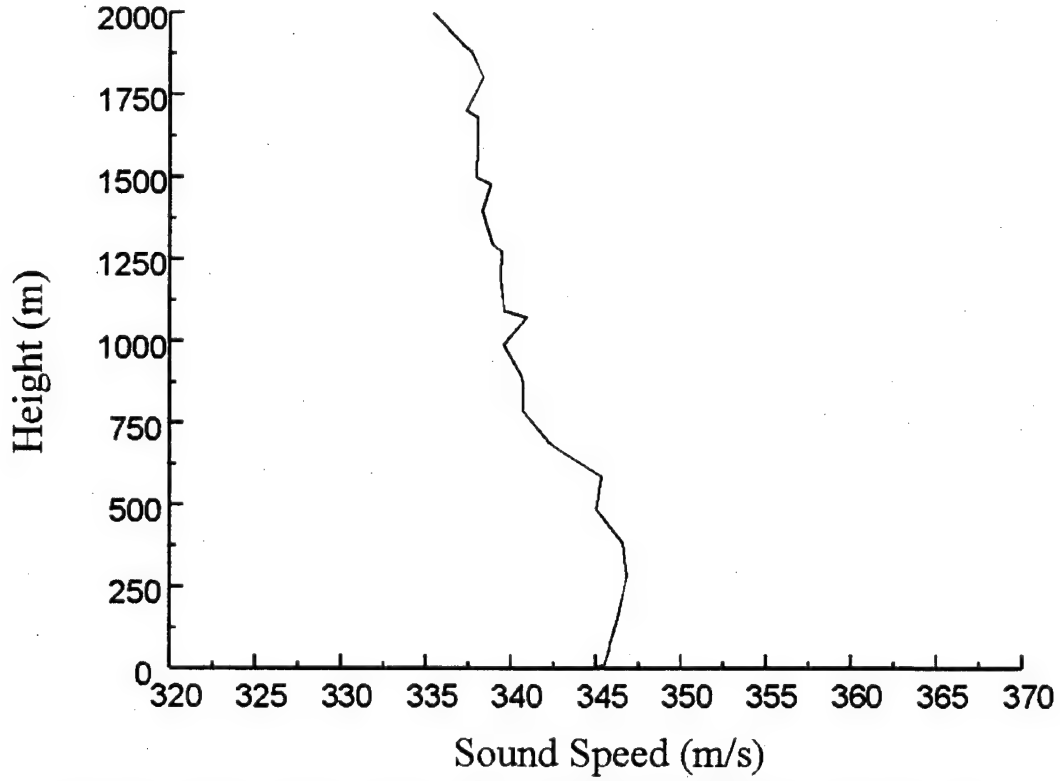

Figure A-4. Sound speed profile along mean bearing to helicopter for Run #1.

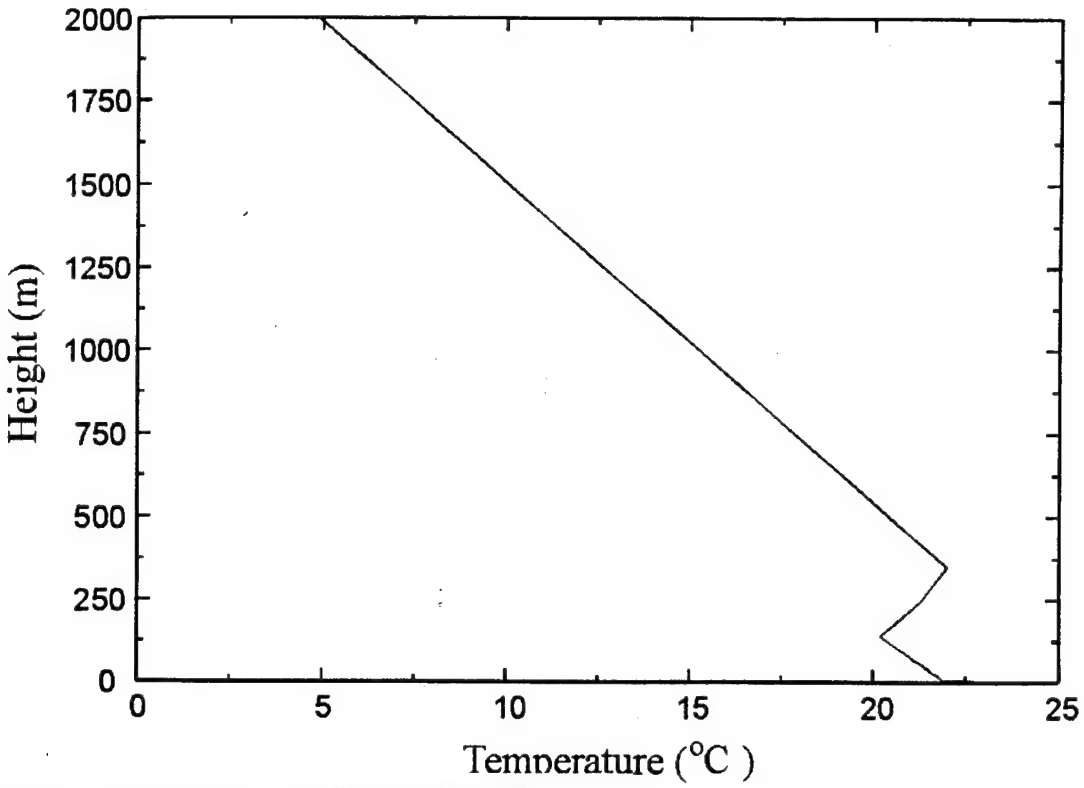

Figure A-5. Temperature profile for Run #2.

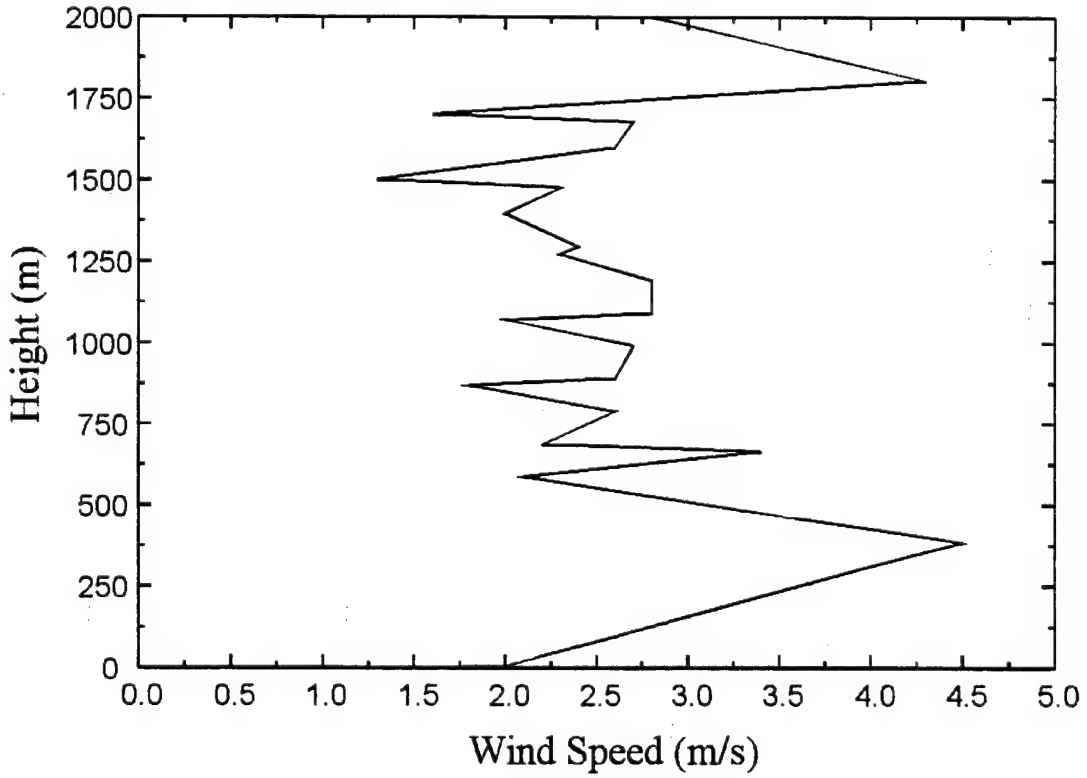

Figure A-6. Wind speed profile for Run #2.

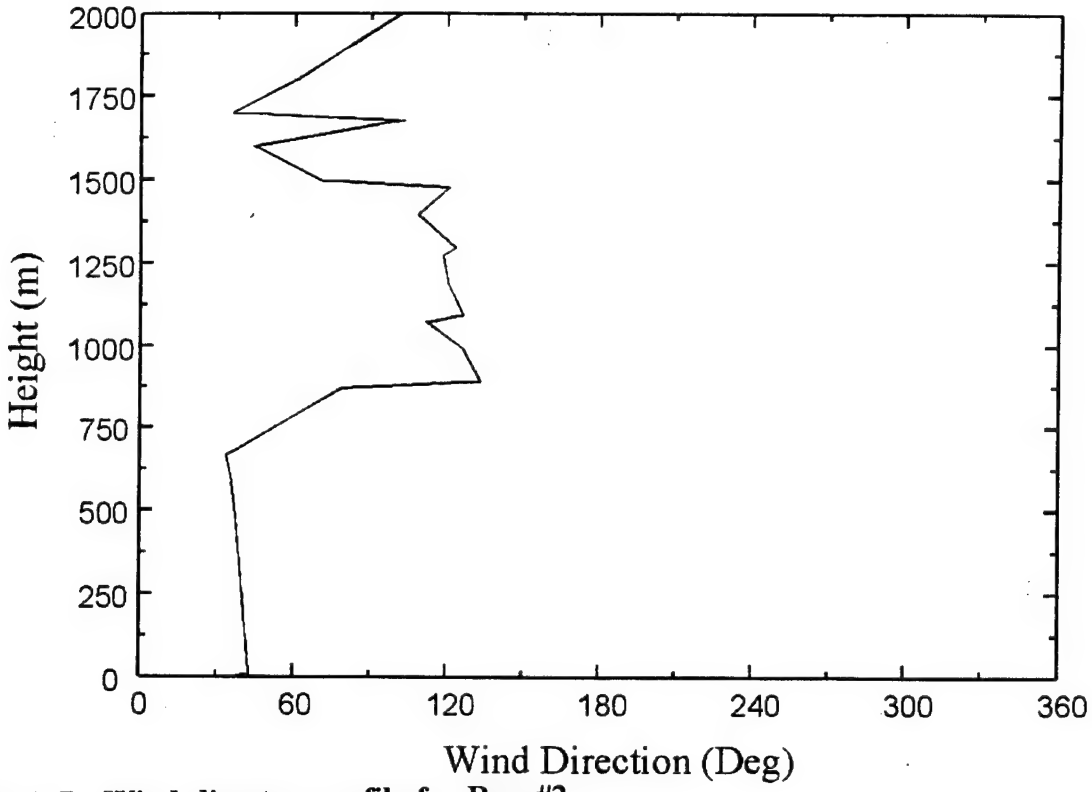

Figure A-7. Wind directon profile for Run #2.

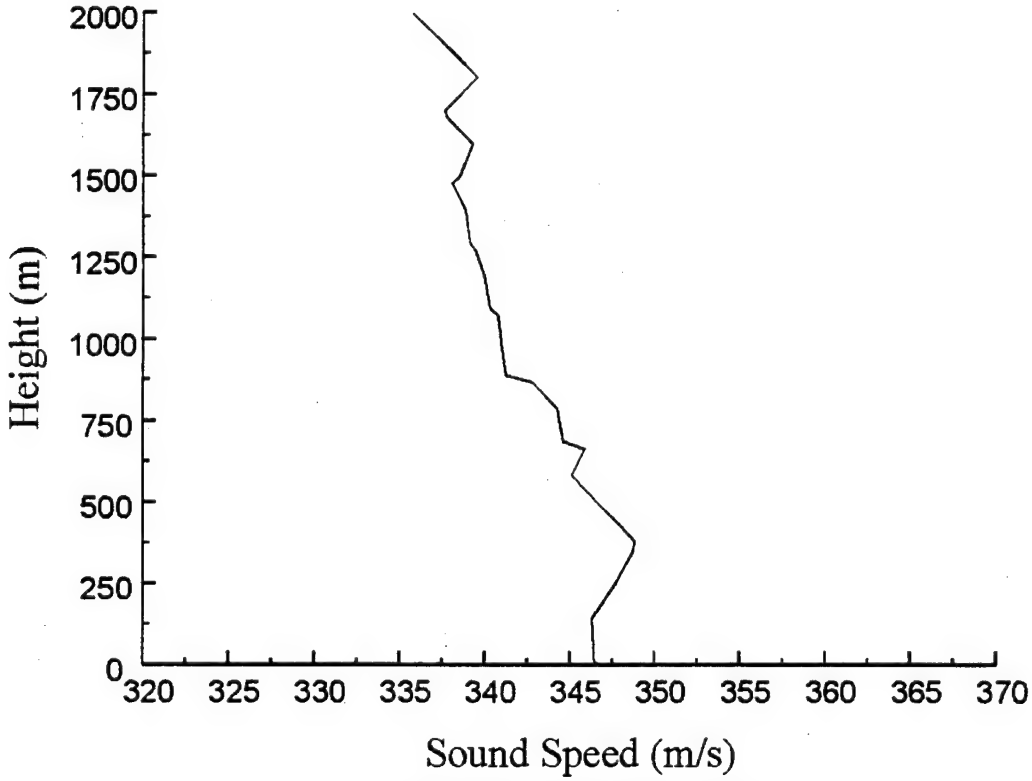

Figure A-8. Sound speed profile along mean bearing to helicopter for Run #2.

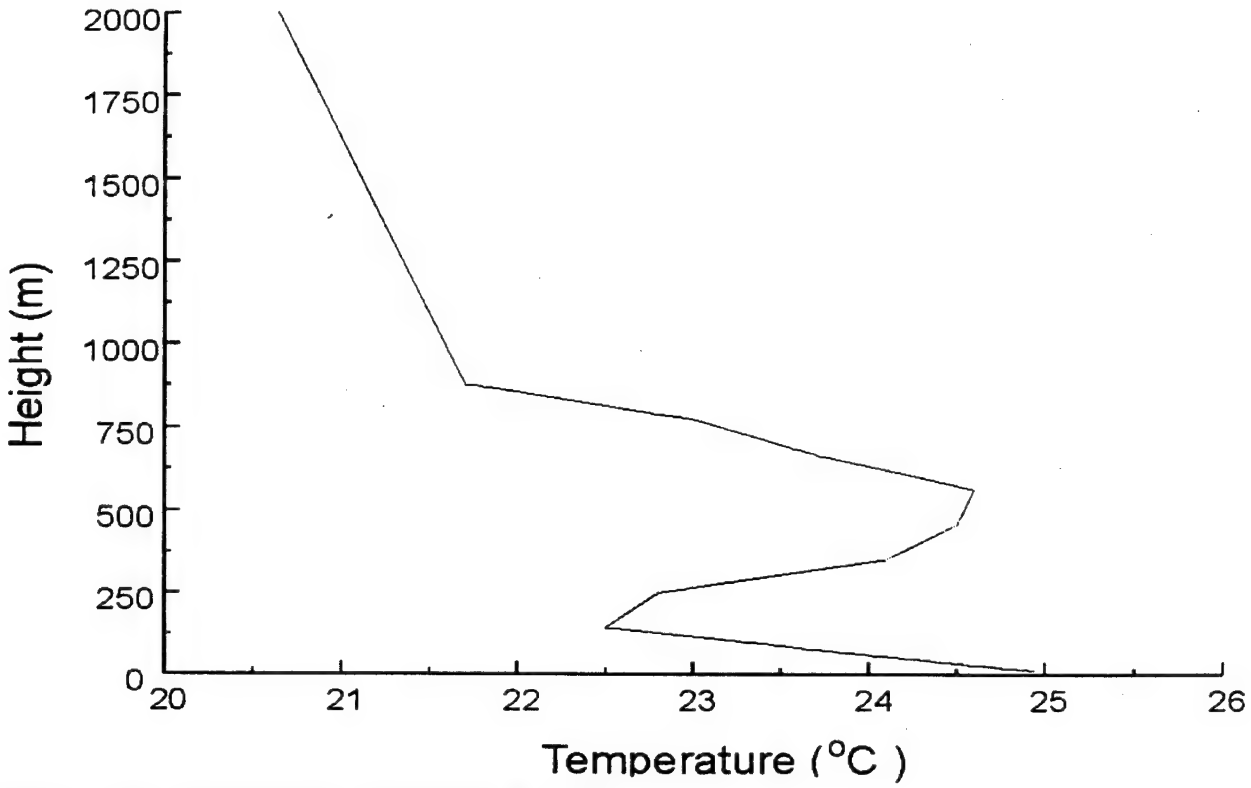

Figure A-9. Temperature profile for Run #3.

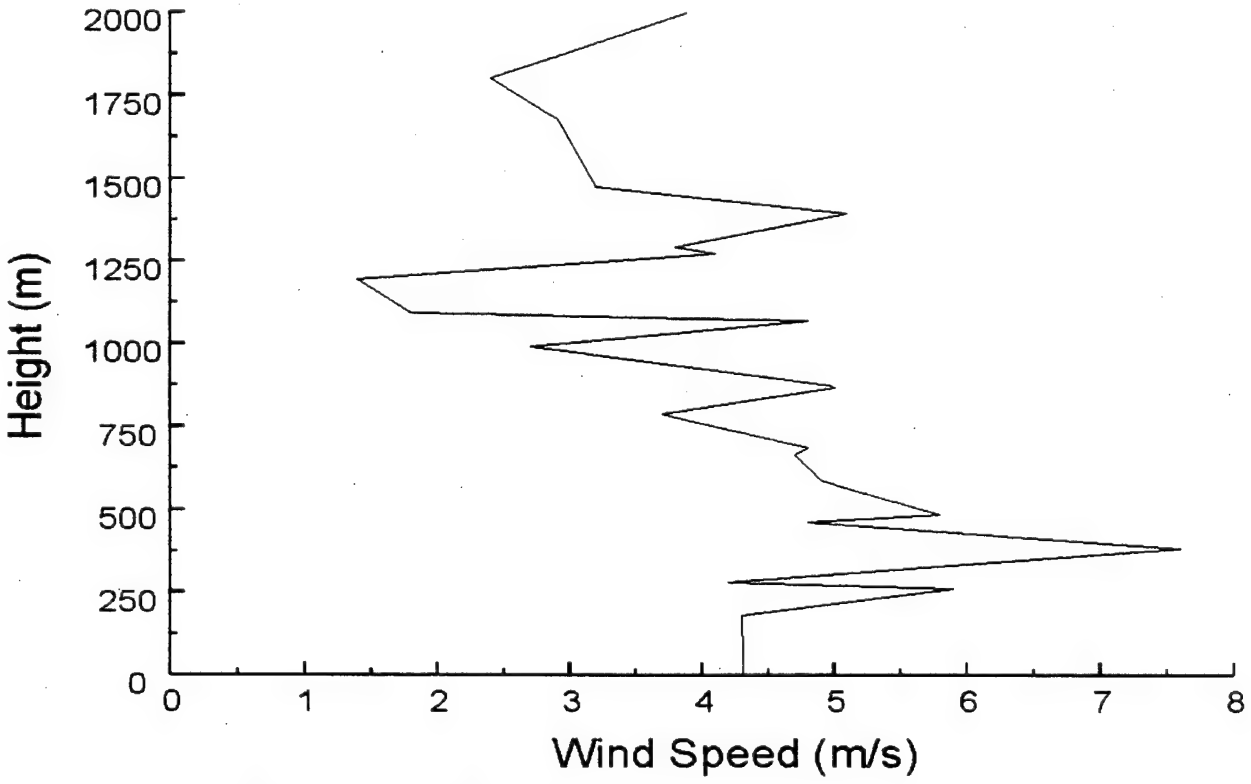

Figure A-10. Wind speed profile for Run #3.

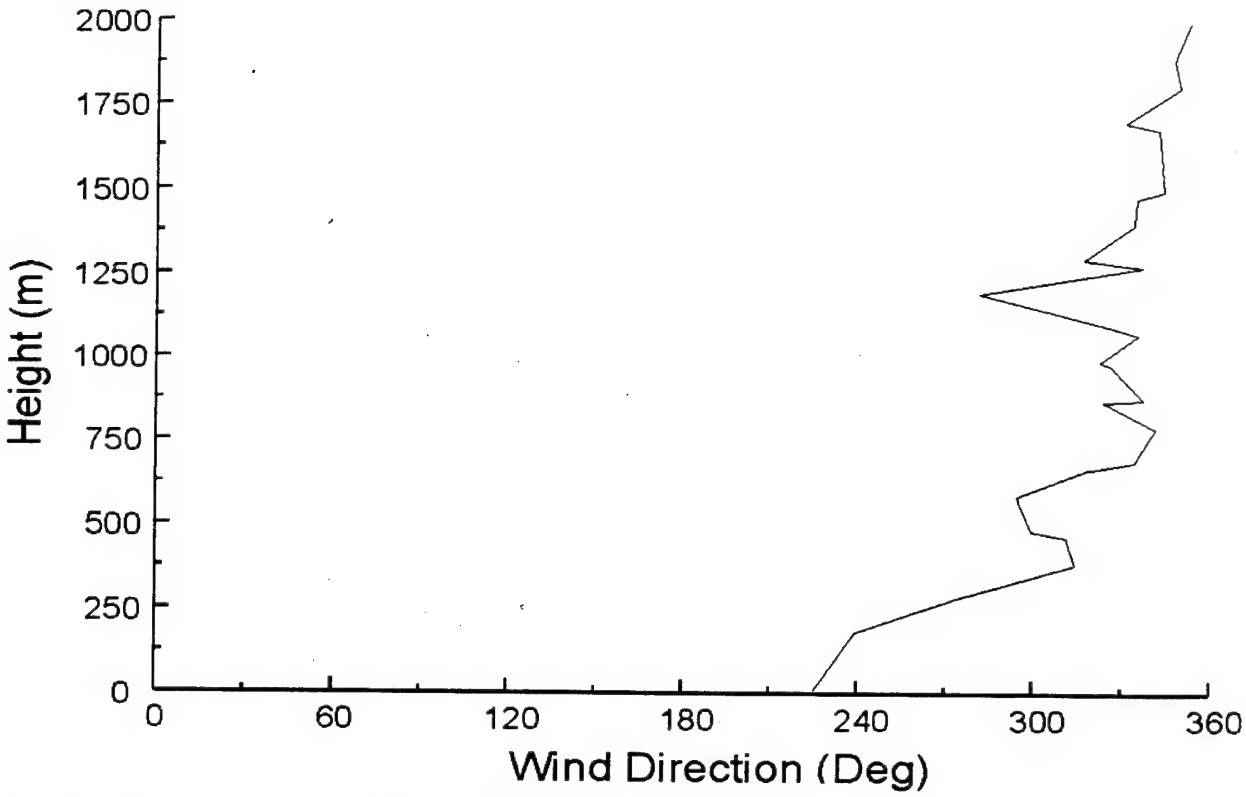

Figure A-11. Wind directon profile for Run #3.

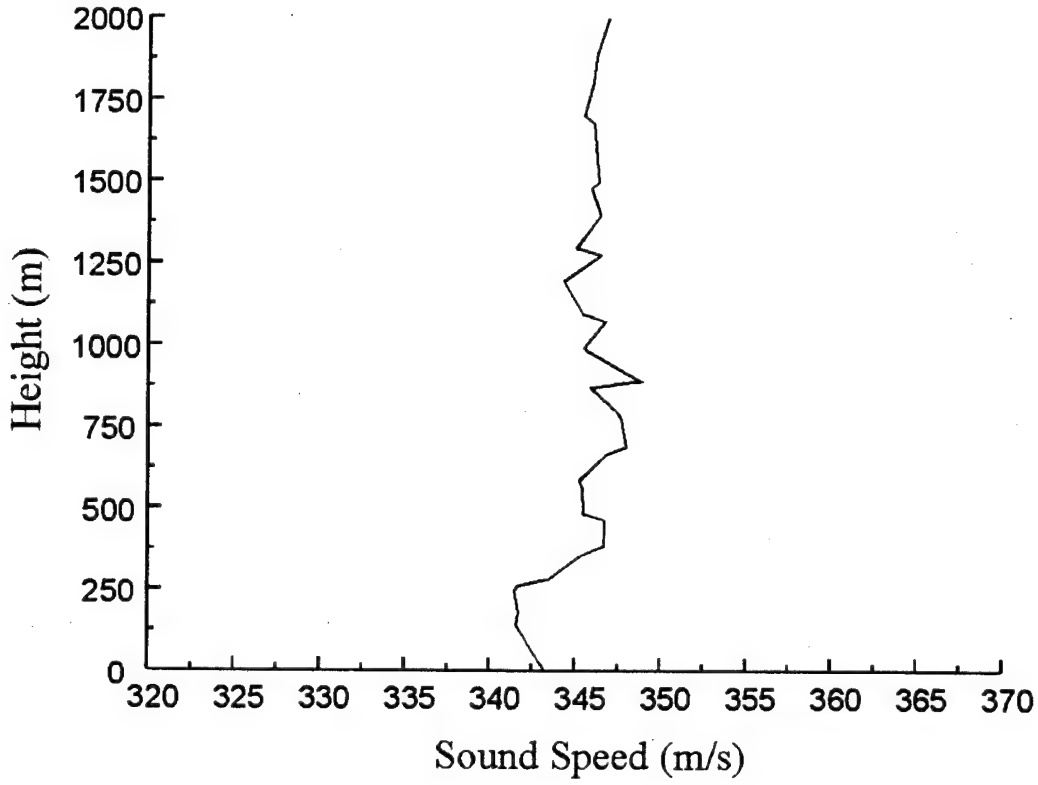

Figure A-12. Sound speed profile along mean bearing to helicopter for Run #3.

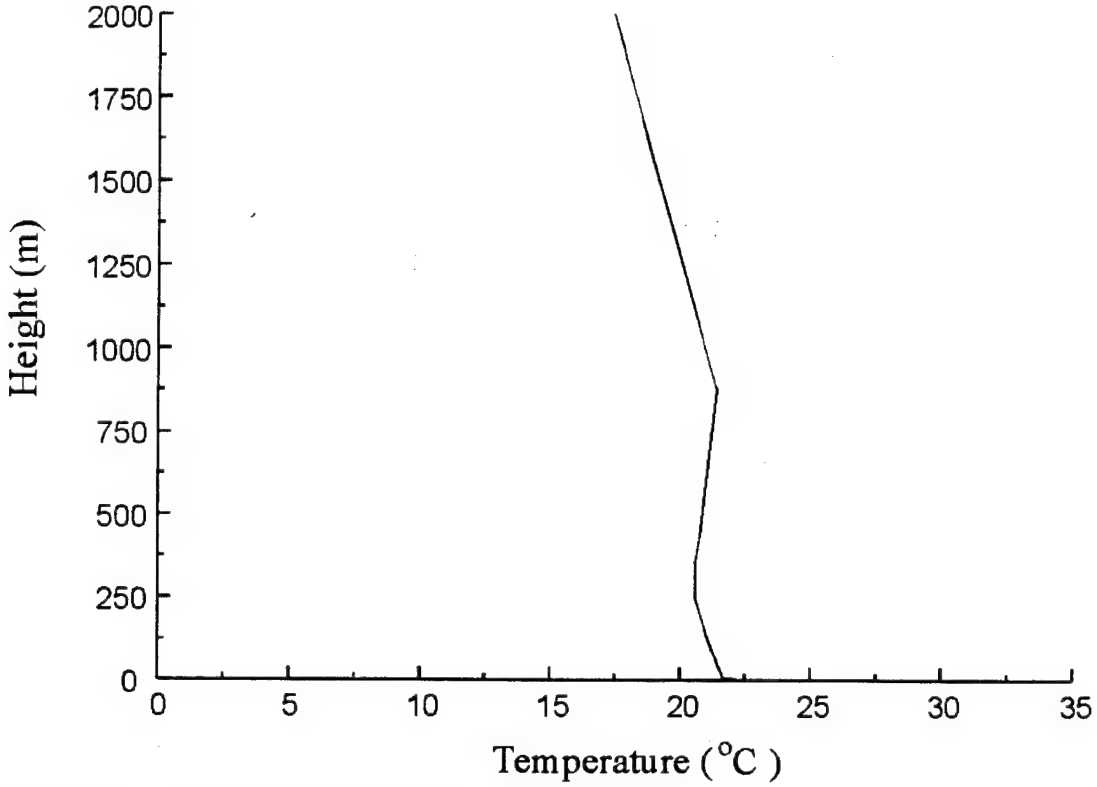

Figure A-13. Temperature profile for Run #4.

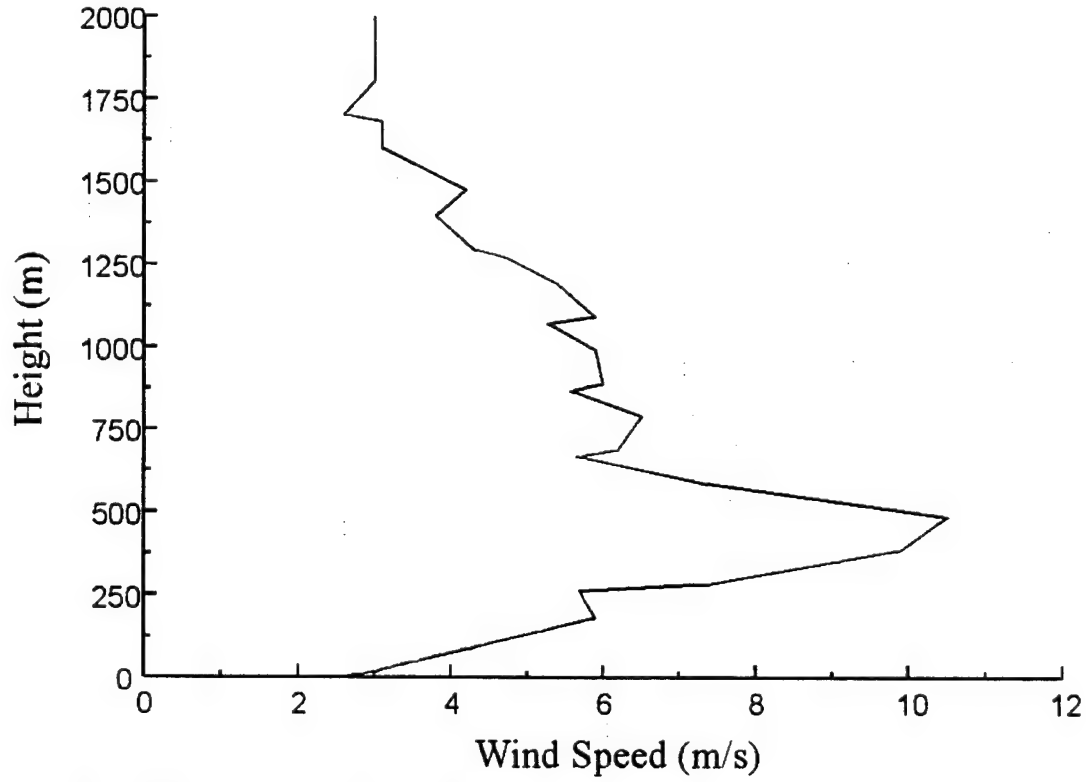

Figure A-14. Wind speed profile for Run #4.

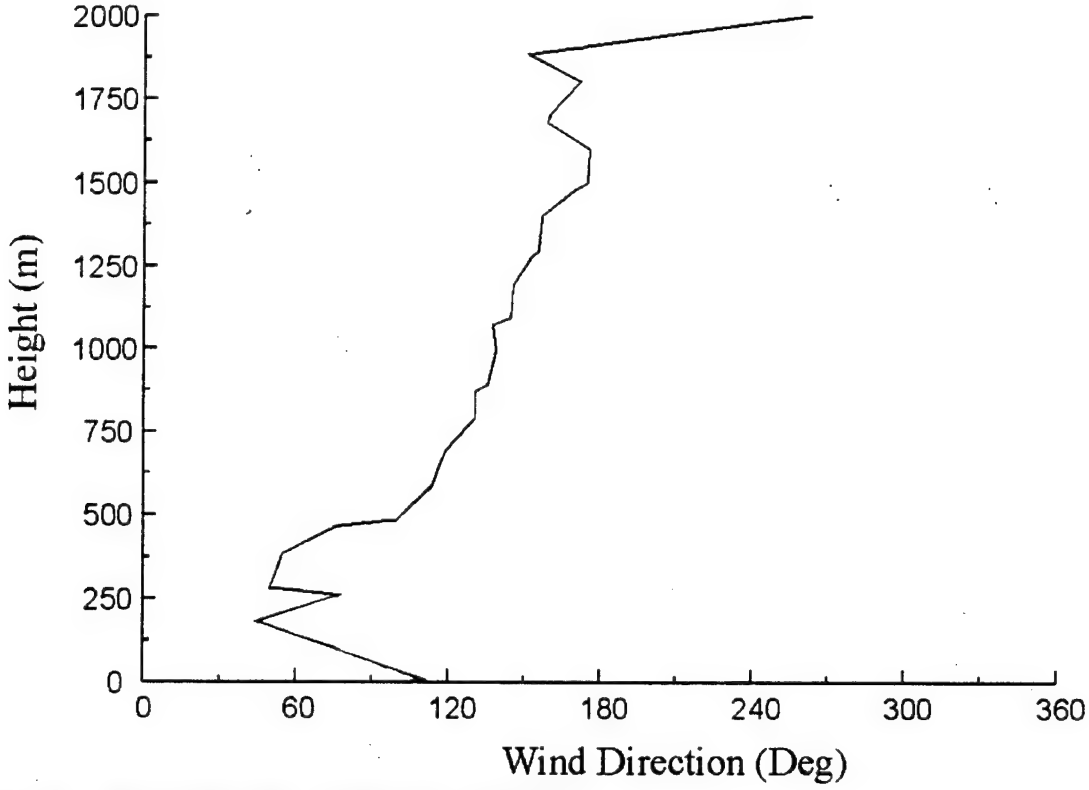

Figure A-15. Wind directon profile for Run #4.

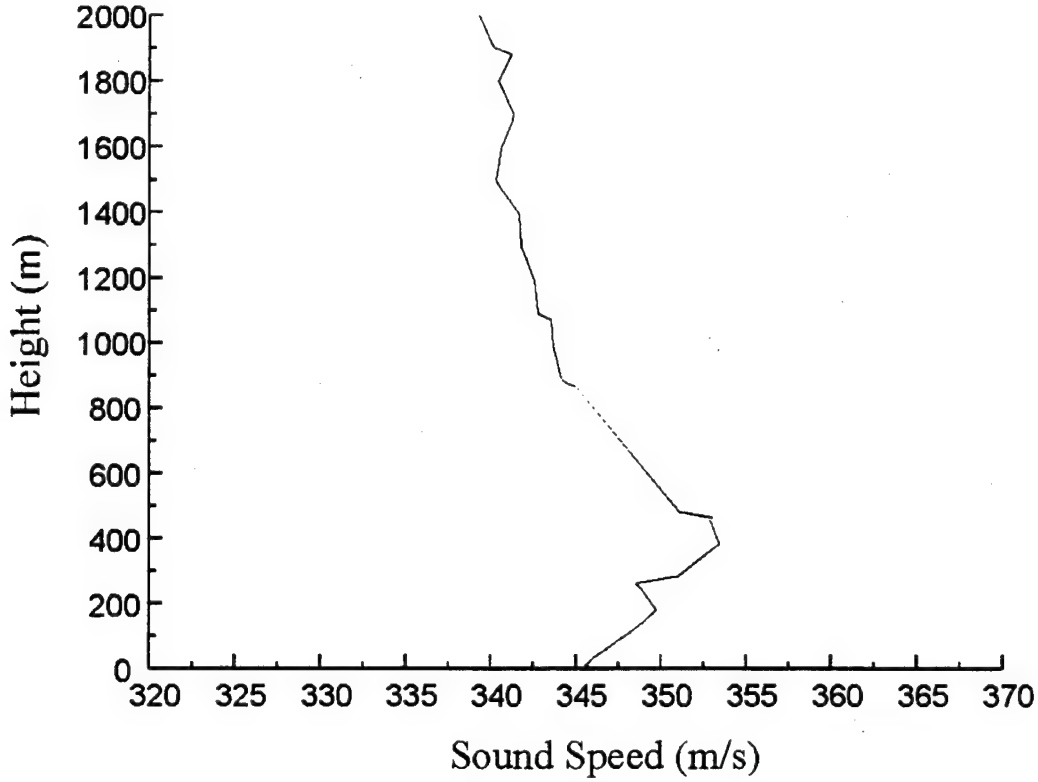

Figure A-16 Sound speed profile along mean bearing to helicopter for Run #4.

Appendix B

Helicopter Track For Each Comparison

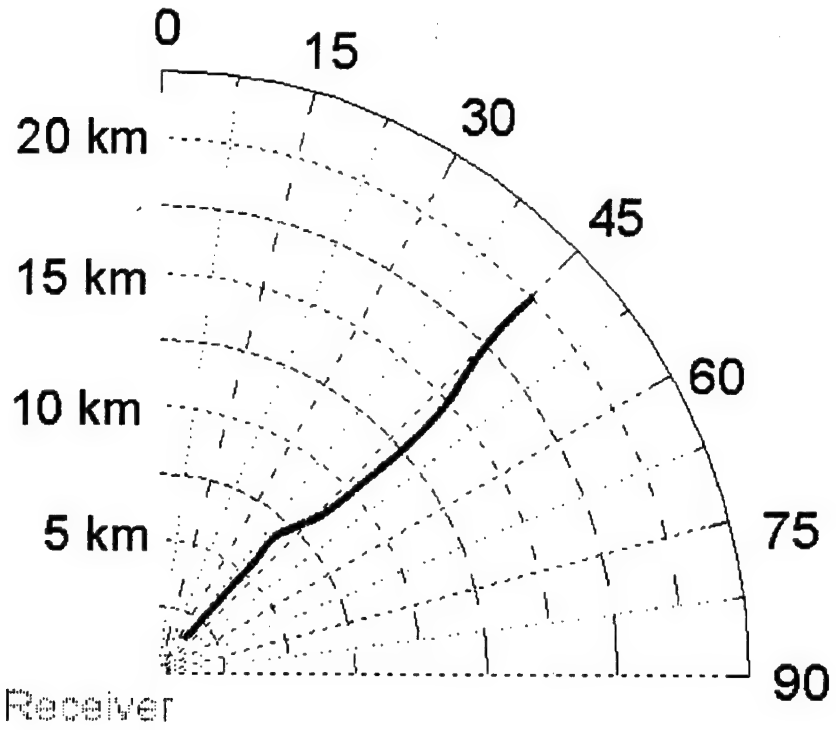

Figure B-1. Track of helicopter for Run #1.

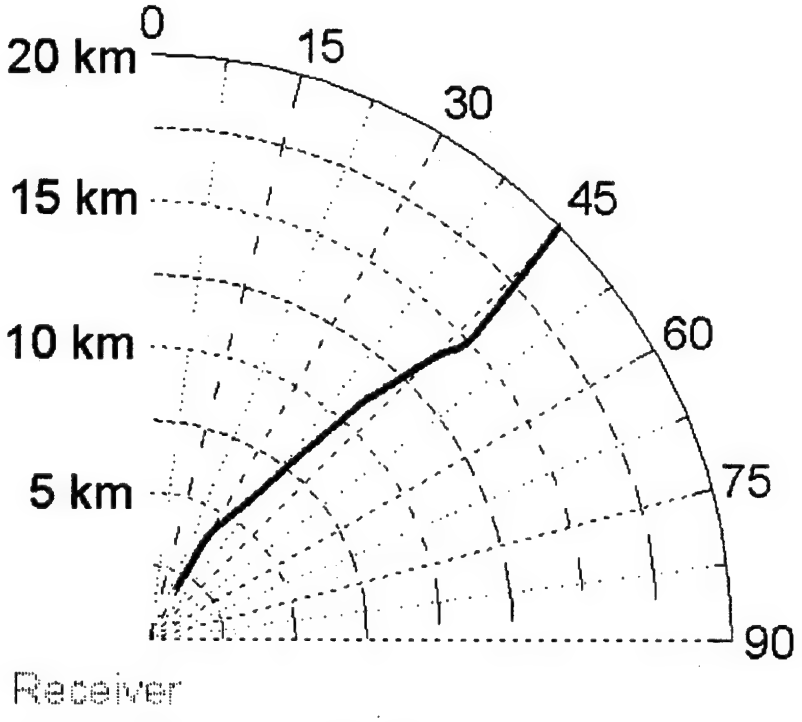

Figure B-2. Track of helicopter for Run #2.

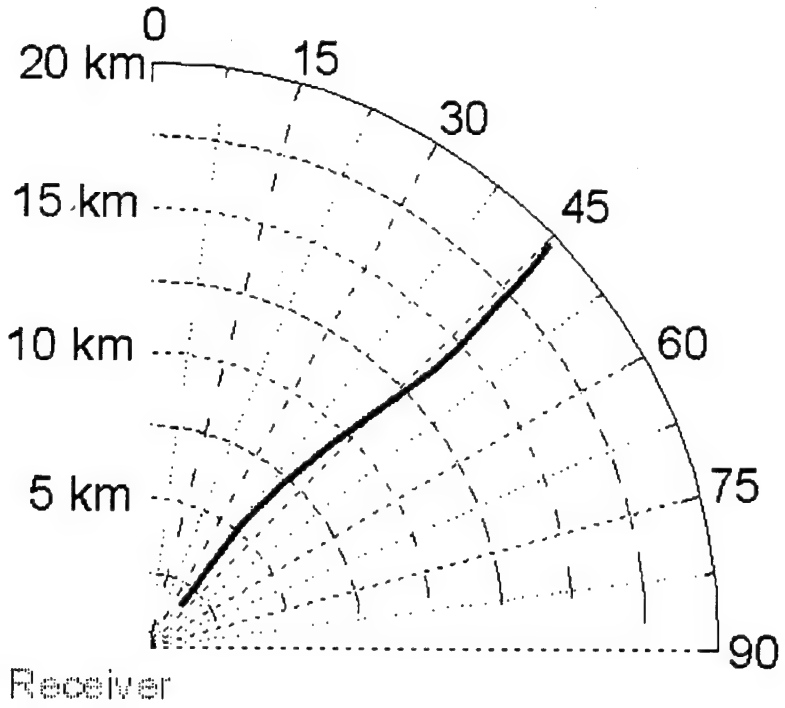

Figure B-3. Track of helicopter for Run #3.

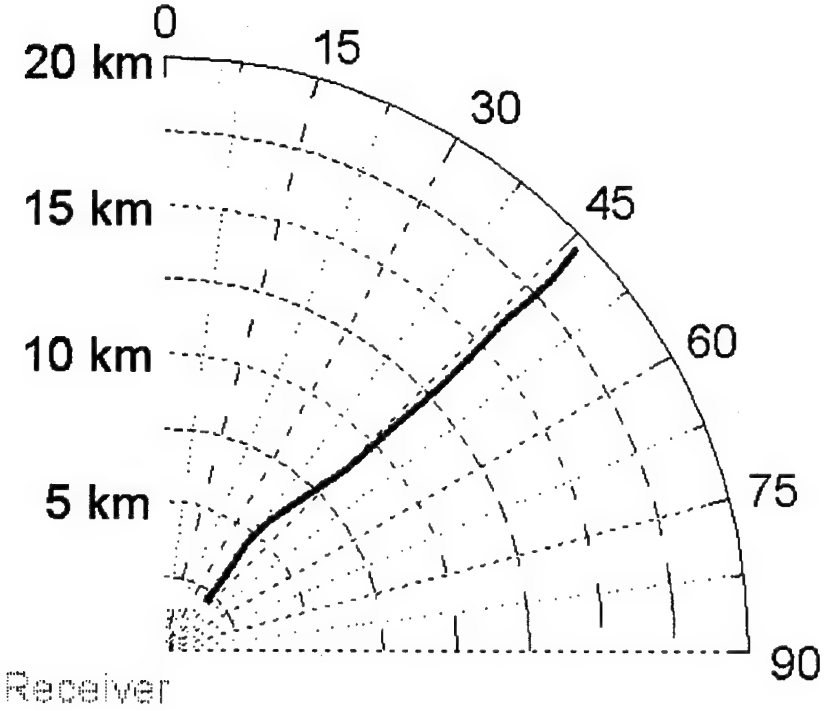

Figure B-4. Track of helicopter for Run #4.

Appendix C

Example Set of Plots For Each Comparison

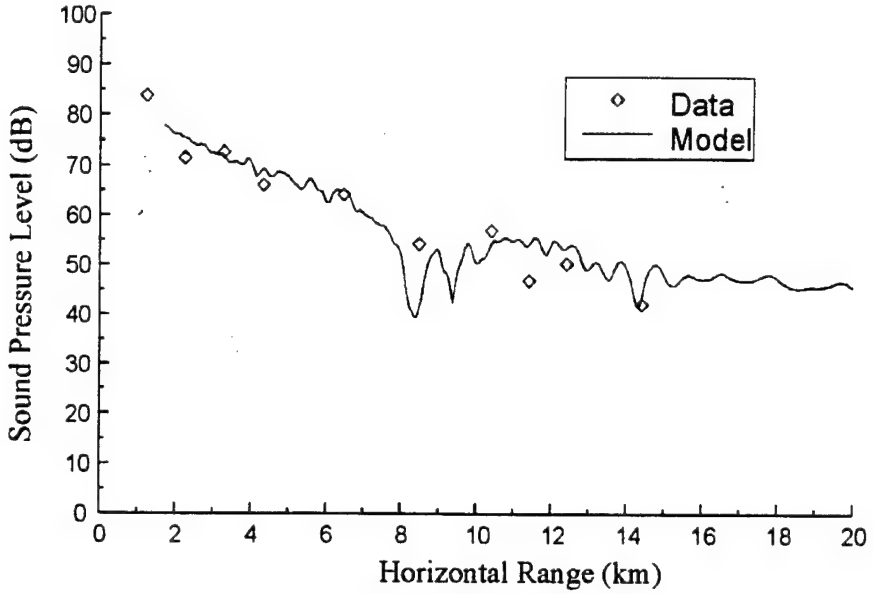

Figure C-1. Comparison between SCAFFIP and helicopter data for Run #1 and 21 Hz.

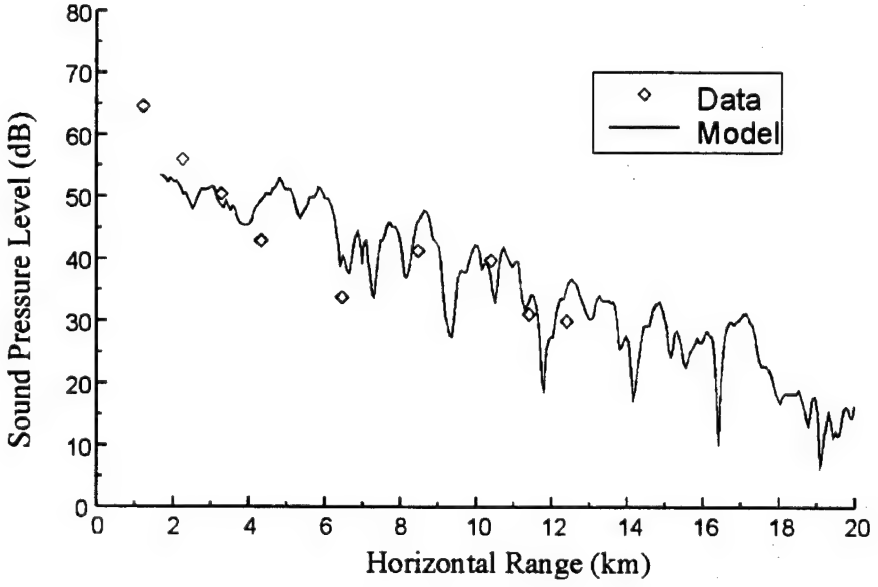

Figure C-2. Comparison between SCAFFIP and helicopter data for Run #1 and 124 Hz.

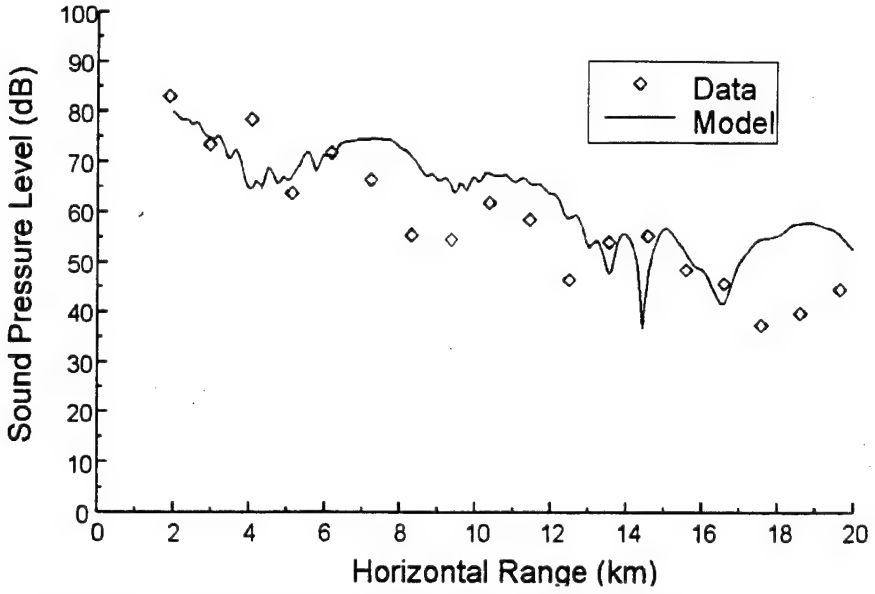

Figure C-3. Comparison between SCAFFIP and helicopter data for Run #2 and 21 Hz.

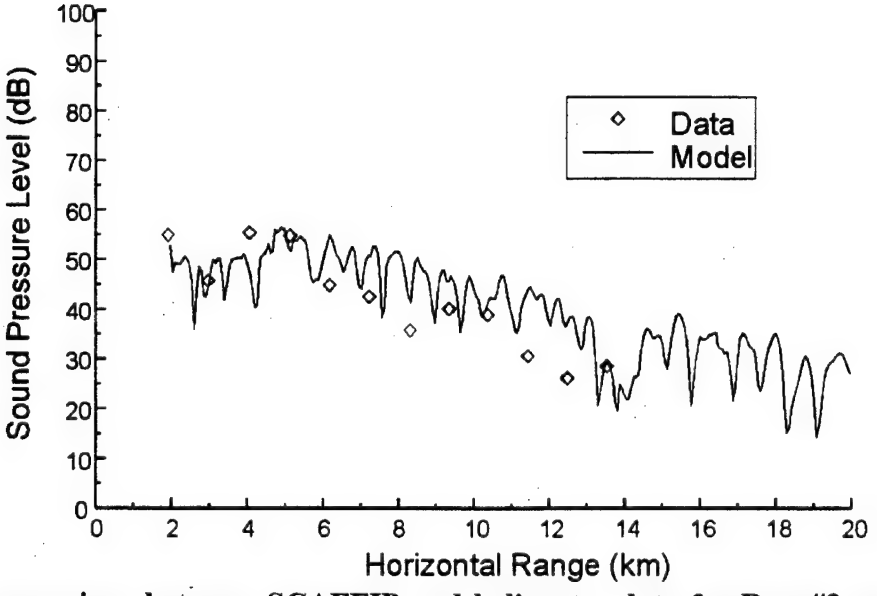

Figure C-4. Comparison between SCAFFIP and helicopter data for Run #2 and 124 Hz.

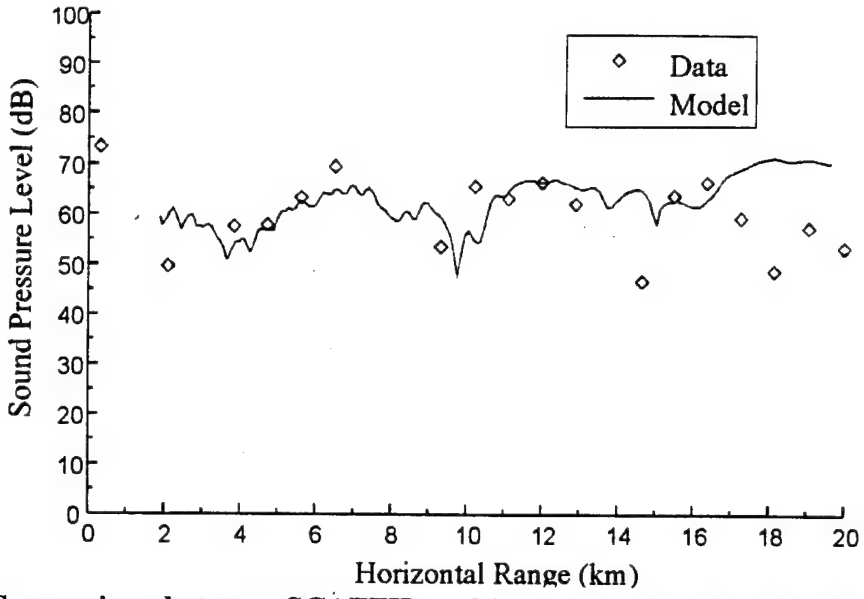

Figure C-5. Comparison between SCAFFIP and helicopter data for Run #3 and 23 Hz.

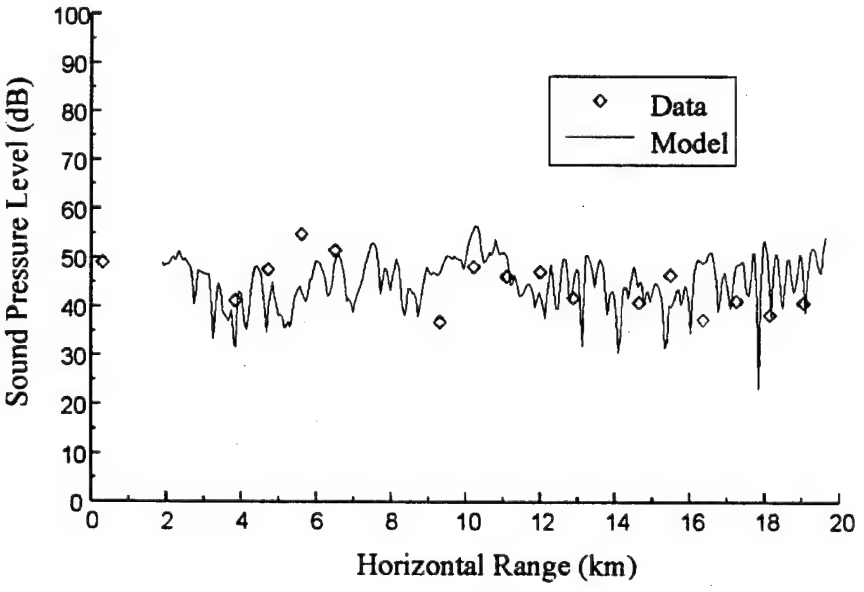

Figure C-6. Comparison between SCAFFIP and helicopter data for Run #3 and 113 Hz.

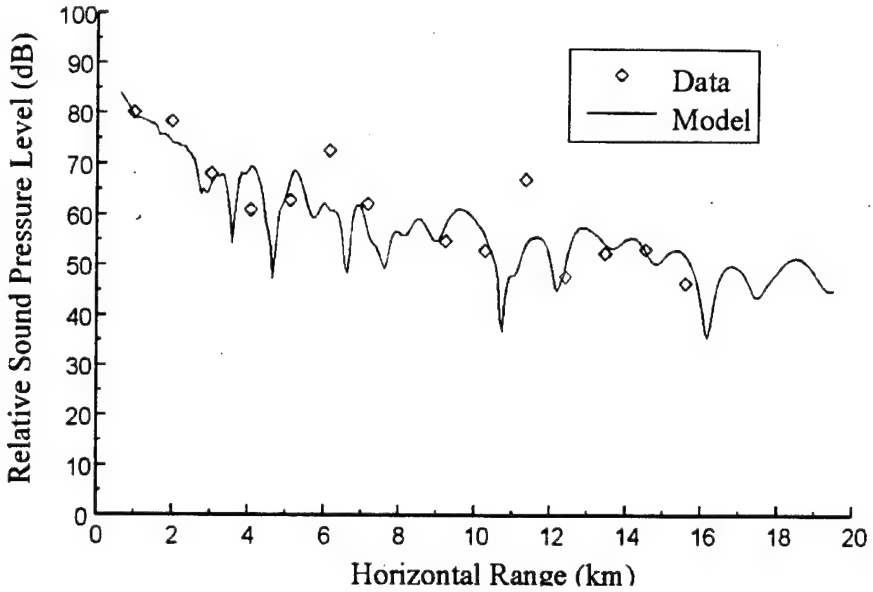

Figure C-7. Comparison between SCAFFIP and helicopter data for Run #4 and 21 Hz.

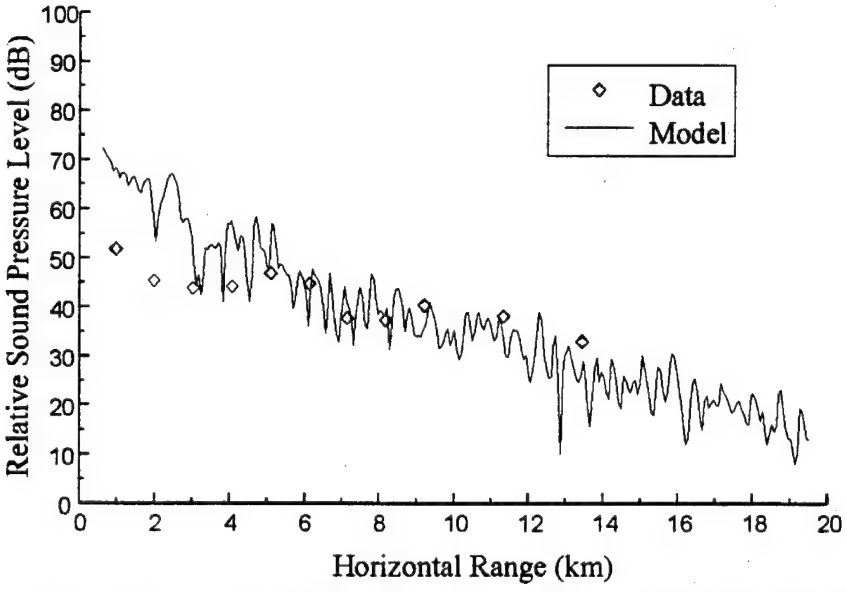

Figure C-8. Comparison between SCAFFIP and helicopter data for Run #4 and 124 Hz.

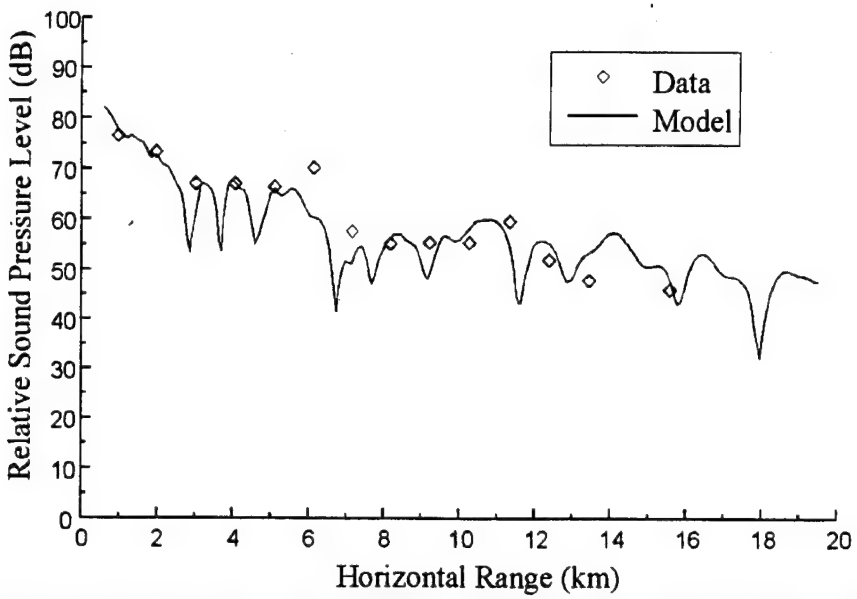

Figure C-9. Comparison between SCAFFIP and helicopter data for Run #4 and 23 Hz.

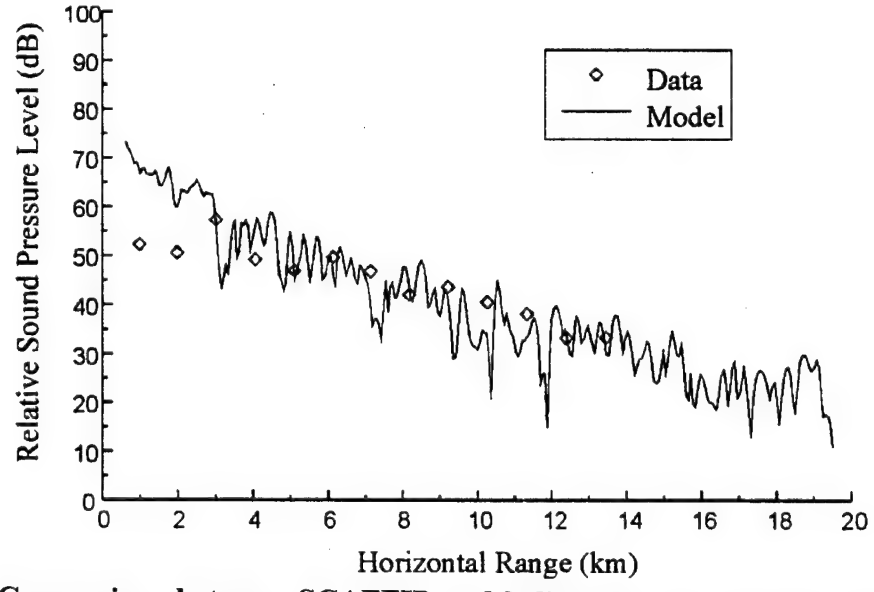

Figure C-10. Comparison between SCAFFIP and helicopter data for Run #4 and 113 Hz.

Distribution

	Copies
NASA MARSHAL SPACE FLT CTR ATMOSPHERIC SCIENCES DIV E501 ATTN DR FICHTL HUNTSVILLE AL 35802	1
NASA SPACE FLT CTR ATMOSPHERIC SCIENCES DIV CODE ED 41 1 HUNTSVILLE AL 35812	1
ARMY STRAT DEFNS CMND CSSD SL L ATTN DR LILLY PO BOX 1500 HUNTSVILLE AL 35807-3801	1
ARMY MISSILE CMND AMSMI RD AC AD ATTN DR PETERSON REDSTONE ARSENAL AL 35898-5242	1
ARMY MISSILE CMND AMSMI RD AS SS ATTN MR H F ANDERSON REDSTONE ARSENAL AL 35898-5253	1
ARMY MISSILE CMND AMSMI RD AS SS ATTN MR B WILLIAMS REDSTONE ARSENAL AL 35898-5253	1
ARMY MISSILE CMND AMSMI RD DE SE ATTN MR GORDON LILL JR REDSTONE ARSENAL AL 35898-5245	1

ARMY MISSILE CMND 1
REDSTONE SCI INFO CTR
AMSMI RD CS R DOC
REDSTONE ARSENAL
AL 35898-5241

ARMY MISSILE CMND 1
AMSMI
REDSTONE ARSENAL
AL 35898-5253

ARMY INTEL CTR 1
AND FT HUACHUCA
ATSI CDC C
FT HUACHUCA AZ 85613-7000

CMD (420000D(C0245)) 1
ATTN DR A SHLANTA
NAVAIRWARCENWPNDIV
1 ADMIN CIR
CHINA LAKE CA 93555-6001

PACIFIC MISSILE TEST CTR 1
GEOPHYSICS DIV
ATTN CODE 3250
POINT MUGU CA 93042-5000

LOCKHEED MIS & SPACE CO 1
ATTN KENNETH R HARDY
ORG 91 01 B 255
3251 HANOVER STREET
PALO ALTO CA 94304-1191

NAVAL OCEAN SYST CTR 1
CODE 54
ATTN DR RICHTER
SAN DIEGO CA 92152-5000

METEOROLOGIST IN CHARGE 1
KWAJALEIN MISSILE RANGE
PO BOX 67
APO SAN FRANCISCO
CA 96555

DEPT OF COMMERCE CTR 1
MOUNTAIN ADMINISTRATION
SPPRT CTR LIBRARY R 51
325 S BROADWAY
BOULDER CO 80303

DR HANS J LIEBE 1
NTIA ITS S 3
325 S BROADWAY
BOULDER CO 80303

NCAR LIBRARY SERIALS 1
NATL CTR FOR ATMOS RSCH
PO BOX 3000
BOULDER CO 80307-3000

DEPT OF COMMERCE CTR 1
325 S BROADWAY
BOULDER CO 80303

DAMI POI 1
WASH DC 20310-1067

MIL ASST FOR ENV SCI OFC 1
OF THE UNDERSEC OF DEFNS
FOR RSCH & ENGR R&AT E LS
PENTAGON ROOM 3D129
WASH DC 20301-3080

DEAN RMD 1
ATTN DR GOMEZ
WASH DC 20314

ARMY INFANTRY 1
ATSH CD CS OR
ATTN DR E DUTOIT
FT BENNING GA 30905-5090

AIR WEATHER SERVICE 1
TECH LIBRARY FL4414 3
SCOTT AFB IL 62225-5458

USAFETAC DNE 1
ATTN MR GLAUBER
SCOTT AFB IL 62225-5008

HQ AWS DOO 1 1
SCOTT AFB IL 62225-5008

PHILLIPS LABORATORY 1
PL LYP
ATTN MR CHISHOLM
HANSCOM AFB MA 01731-5000

ATMOSPHERIC SCI DIV 1
GEOPHYSICS DIRCTRT
PHILLIPS LABORATORY
HANSCOM AFB MA 01731-5000

PHILLIPS LABORATORY 1
PL LYP 3
HANSCOM AFB MA 01731-5000

RAYTHEON COMPANY 1
ATTN DR SONNENSCHEIN
528 BOSTON POST ROAD
SUDBURY MA 01776
MAIL STOP 1K9

ARMY MATERIEL SYST 1
ANALYSIS ACTIVITY
AMXSY
ATTN MP H COHEN
APG MD 21005-5071

ARMY MATERIEL SYST 1
ANALYSIS ACTIVITY
AMXSY AT
ATTN MR CAMPBELL
APG MD 21005-5071

ARMY MATERIEL SYST 1
ANALYSIS ACTIVITY
AMXSY CR
ATTN MR MARCHET
APG MD 21005-5071

ARL CHEMICAL BIOLOGY
NUC EFFECTS DIV
AMSRL SL CO
APG MD 21010-5423 1

ARMY MATERIEL SYST
ANALYSIS ACTIVITY
AMXSY
APG MD 21005-5071 1

ARMY MATERIEL SYST
ANALYSIS ACTIVITY
AMXSY CS
ATTN MR BRADLEY
APG MD 21005-5071 1

ARMY RESEARCH LABORATORY
AMSRL D
2800 POWDER MILL ROAD
ADELPHI MD 20783-1145 1

ARMY RESEARCH LABORATORY
AMSRL OP SD TP
TECHNICAL PUBLISHING
2800 POWDER MILL ROAD
ADELPHI MD 20783-1145 1

ARMY RESEARCH LABORATORY
AMSRL OP CI SD TL
2800 POWDER MILL ROAD
ADELPHI MD 20783-1145 1

ARMY RESEARCH LABORATORY
AMSRL SS SH
ATTN DR SZTANKAY
2800 POWDER MILL ROAD
ADELPHI MD 20783-1145 1

ARMY RESEARCH LABORATORY
AMSRL
2800 POWDER MILL ROAD
ADELPHI MD 20783-1145 1

NATIONAL SECURITY AGCY W21 1
ATTN DR LONGBOTHUM
9800 SAVAGE ROAD
FT GEORGE G MEADE
MD 20755-6000

OIC NAVSWC 1
TECH LIBRARY CODE E 232
SILVER SPRINGS
MD 20903-5000

ARMY RSRC OFC 1
ATTN AMXRO GS (DR BACH)
PO BOX 12211
RTP NC 27009

DR JERRY DAVIS 1
NCSU
PO BOX 8208
RALEIGH NC 27650-8208

US ARMY CECRL 1
CECRL GP
ATTN DR DETSCH
HANOVER NH 03755-1290

ARMY ARDEC 1
SMCAR IMI I BLDG 59
DOVER NJ 07806-5000

ARMY SATELLITE COMM AGCY 1
DRCPM SC 3
FT MONMOUTH NJ 07703-5303

ARMY COMMUNICATIONS 1
ELECTR CTR FOR EW RSTA
AMSEL EW D
FT MONMOUTH NJ 07703-5303

ARMY COMMUNICATIONS 1
ELECTR CTR FOR EW RSTA
AMSEL EW MD
FT MONMOUTH NJ 07703-5303

ARMY DUGWAY PROVING GRD
STEDP MT DA L 3
DUGWAY UT 84022-5000 1

ARMY DUGWAY PROVING GRD
STEDP MT M
ATTN MR BOWERS
DUGWAY UT 84022-5000 1

DEPT OF THE AIR FORCE
OL A 2D WEATHER SQUAD MAC
HOLLOMAN AFB
NM 88330-5000 1

PL WE
KIRTLAND AFB NM
87118-6008 1

USAF ROME LAB TECH
CORRIDOR W STE 262 RL SUL
26 ELECTR PKWY BLD 106
GRIFFISS AFB
NY 13441-4514 1

AFMC DOW
WRIGHT PATTERSON AFB
OH 0334-5000 1

ARMY FIELD ARTLLRY SCHOOL
ATSF TSM TA
FT SILL OK 73503-5600 1

NAVAL AIR DEV CTR
CODE 5012
ATTN AL SALIK
WARMINISTER PA 18974 1

ARMY FOREGN SCI TECH CTR
CM
220 7TH STREET NE
CHARLOTTESVILLE
VA 22901-5396 1

NAVAL SURFACE WEAPONS CTR 1
CODE G63
DAHLGREN VA 22448-5000

ARMY OEC 1
CSTE EFS
PARK CENTER IV
4501 FORD AVE
ALEXANDRIA VA 22302-1458

ARMY CORPS OF ENGRS 1
ENGR TOPOGRAPHICS LAB
ETL GS LB
FT BELVOIR VA 22060

ARMY TOPO ENGR CTR 1
CETEC ZC 1
FT BELVOIR VA 22060-5546

LOGISTICS CTR 1
ATCL CE
FT LEE VA 23801-6000

SCI AND TECHNOLOGY 1
101 RESEARCH DRIVE
HAMPTON VA 23666-1340

ARMY NUCLEAR CML AGCY 1
MONA ZB BLDG 2073
SPRINGFIELD VA 22150-3198

USATRADOC 1
ATCD FA
FT MONROE VA 23651-5170

ARMY TRADOC ANALYSIS CTR 1
ATRC WSS R
WSMR NM 88002-5502

ARMY RESEARCH LABORATORY 1
AMSRL BE S
BATTLEFIELD ENVIR DIR
WSMR NM 88002-5501

ARMY RESEARCH LABORATORY AMSRL BE E BATTLEFIELD ENVIR DIR WSMR NM 88002-5501	1
ARMY RESEARCH LABORATORY AMSRL BE W BATTLEFIELD ENVIR DIR WSMR NM 88002-5501	1
ARMY RESEARCH LABORATORY AMSRL BE ATTN MR VEAZY BATTLEFIELD ENVIR DIR WSMR NM 88002-5501	1
DTIC 8725 JOHN J. KINGMAN RD STE 0944 FT BELVOIR VA 22060-6218	1
ARMY MISSILE CMND AMSMI REDSTONE ARSENAL AL 35898-5243	1
ARMY DUGWAY PROVING GRD STEDP 3 DUGWAY UT 84022-5000	1
USATRADOC ATCD FA FT MONROE VA 23651-5170	1
WSMR TECH LIBRARY BR STEWS IM IT WSMR NM 88001	1
Record Copy	2
TOTAL	79